Double Horizon Model-Based Policy Optimization

Anonymous authors
Paper under double-blind review

Abstract

Model-based reinforcement learning (MBRL) reduces the cost of real-environment sampling by generating synthetic trajectories (called rollouts) from a learned dynamics model. However, choosing the length of the rollouts poses two dilemmas: (1) Longer rollouts better preserve on-policy training but amplify model bias, indicating the need for an intermediate horizon to mitigate distribution shift (i.e., the gap between on-policy and past off-policy samples). (2) Moreover, a longer model rollout may reduce value estimation bias but raise the variance of policy gradients due to backpropagation through multiple steps, implying another intermediate horizon for stable gradient estimates. However, these two optimal horizons may differ. To resolve this conflict, we propose Double Horizon Model-Based Policy Optimization (DHMBPO), which divides the rollout procedure into a long "distribution rollout" (DR) and a short "training rollout" (TR). The DR generates on-policy state samples for mitigating distribution shift. In contrast, the short TR leverages differentiable transitions to offer accurate value gradient estimation with stable gradient updates, thereby requiring fewer updates and reducing overall runtime. We demonstrate that the double-horizon approach effectively balances distribution shift, model bias, and gradient instability, and surpasses existing MBRL methods on continuous-control benchmarks in terms of both sample efficiency and runtime.

1 Introduction

Reinforcement learning (RL) is a framework to find a good policy in sequential decision making applications via trial-and-error with an environment. Model-based RL (MBRL), which learns dynamics model of an environment by data-driven manner, leverages the learned dynamics model to generate synthetic samples, reducing costly real-environment interactions. However, if the model is imperfect, long synthetic rollouts can introduce significant errors, a "model bias", especially when the rollout length is large. Additionally, data collected under a poorly performing policy differs from what the current policy would actually encounter, thus there is "distribution shift" for policy evaluation (Hallak and Mannor, 2017) and policy improvement (Liu et al., 2019). Several MBRL methods address these issues by tailoring the length and usage of model's predictions.

Broadly, these successful approaches can be grouped into two types. The first type employs differentiable rollouts (Deisenroth and Rasmussen, 2011; Amos et al., 2021; Hafner et al., 2019; Hansen et al., 2024), or model derivatives on predictions (Zhang et al., 2024). By backpropagating through a few model-predicted transitions, these methods compute a model-based value expansion (MVE) estimator (Feinberg et al., 2018), which sums on-policy rewards for intermediate states with the estimated return from the terminal state or a critic's prediction. Because the MVE estimator refines value estimation, the policy can improve based on more accurate on-policy value estimates even with a lower update-to-data (UTD) ratio, i.e., the number of policy parameter updates per environment step. This lower UTD ratio also helps suppress the increase in computation time (Hiraoka et al., 2022). However, extending differentiable rollouts in conjunction with the reparametrization trick (Kingma and Welling, 2013) can inflate the variance of the policy gradients (Parmas et al., 2018), which limits how long these training rollouts can effectively be. In this work, we refer to the policy gradient computed via differentiable rollouts as the "value gradient," (Heess et al., 2015; Zhang et al., 2024) distinguishing it from the gradient estimated by a purely model-free algorithm (Sutton et al., 1999; Silver et al., 2014).

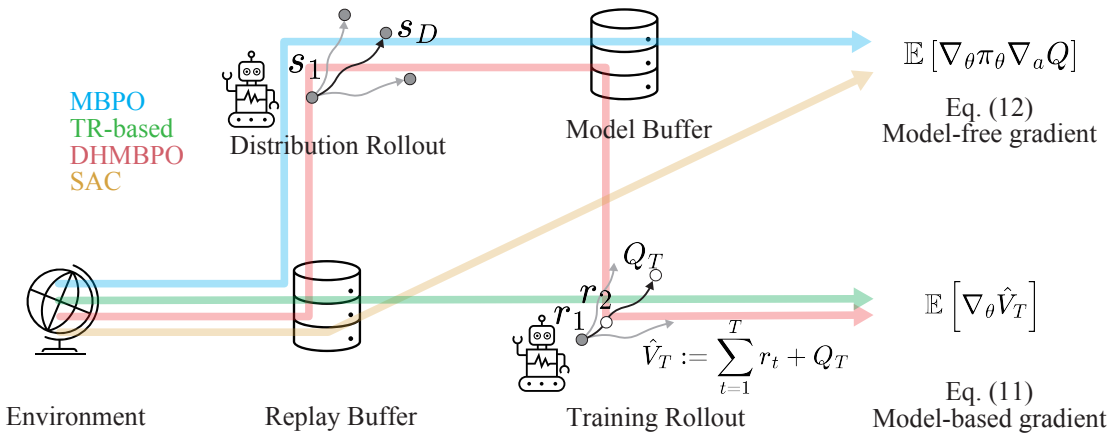

Figure 1: An overview of four approaches to policy gradient estimation: MBPO, TR-based methods, DHMBPO, and an off-policy model-free method. **(1) MBPO (blue lines)** Starts from states in the replay buffer and runs a distribution rollout (DR) with horizon D, generating synthetic samples that are stored in a model buffer. A model-free policy gradient is then computed over these samples. **(2) TR-based (green)** Methods that directly take states from the replay buffer and perform a short-horizon training rollout (TR) with horizon T. A model-based gradient estimate (the value gradient) is then computed. **(3) DHMBPO (red, proposed)** Combines both DR and TR. It first applies a DR on samples from the replay buffer to obtain on-policy samples, which are used as initial states for a short-horizon TR, and then computes the value gradient. **(4) Model-free (yellow)** Represents a fully model-free algorithm that relies solely on replay-buffer data and a model-free gradient estimate.

Meanwhile, another line of MBRL research, the model-based policy optimization (MBPO) algorithm (Janner et al., 2019), adopts a branched rollout approach: starting from states in the replay buffer (which stores states, actions, and rewards), it rolls out a few steps with the learned model to generate synthetic states that more closely match the state distribution of the current policy. MBPO has demonstrated excellent empirical performance in the OpenAI Gym benchmark (Brockman, 2016). Although the MBPO formalization and theoretical analysis do not necessarily support the benefit of model-generated on-policy data, we interpret its empirical success as evidence that optimizing the policy over an on-policy state distribution can improve learning in practice.

In this work, we propose to combine these two ideas: a "distribution rollout" (DR) that approximates the on-policy state distribution (inspired by the branched rollouts in MBPO but without leveraging the differentiability of the predictions), and a "training rollout" (TR) that yields an MVE estimator which does exploit differentiable transitions. However, the optimal horizons for DR and TR may differ. A longer DR helps maintain on-policy samples but also increases model bias, implying an intermediate horizon to minimize distribution shift. On the other hand, a longer TR can reduce value estimation bias but raises the variance of the policy gradients, suggesting another intermediate horizon for stable gradient estimates.

Therefore, we propose different rollout horizons for DR and TR—a long horizon for DR and a short horizon for TR—and name this method the Double Horizon MBPO (DHMBPO) algorithm. In DHMBPO, TR starts from on-policy states provided by the long DR, allowing us to keep the TR horizon short while still achieving adequate value estimation accuracy and effective policy improvement. Figure 1 highlights their concept and the differences.

In experiments on continuous-control benchmarks (Section 4), we show that DHMBPO surpasses existing MBRL methods in sample efficiency and offers lower runtime thanks to a small UTD ratio (Hiraoka et al., 2022). The remainder of this paper presents the necessary background (Section 2), details our approach (Section 3), and provides empirical evaluations demonstrating the benefits of combining these two complementary rollouts.

2 Background

2.1 Notation and Problem Setting

In this work, we consider a Markov decision process (MDP) with entropy regularization (Geist et al., 2019). At each environment step t, an agent in state $s = s_t$ selects an action $a = a_t$ according to a stochastic policy $\pi_\theta(a|s_t)$ parametrized by θ, transitions to the next state s_{t+1} based on the transition probability $p(s|s_t, a_t)$, and receives a reward $r_t = r(s_t, a_t)$. Given a discount factor $\gamma \in [0, 1)$ for weighting future rewards, a distribution $\mu(s)$ from which initial states s_0 are drawn, and a parameter $\alpha \geq 0$ for entropy bonus, the objective is to find a policy parameter to maximize

$$J(\pi) := \mathbb{E}_{s\sim\rho_{\pi_\theta}} \left[V_\alpha^{\pi_\theta}(s) \right], \tag{1}$$

where ρ_{π_θ} is the discounted state visitation distribution under π_θ: $\rho_{\pi_\theta}(s) := (1-\gamma)\sum_{t=0}^{\infty} \gamma^t p(s_t = s|\mu, \pi_\theta)$ and $p(s_t = s|\mu, \pi_\theta)$ is the probability of observing state s at time t with $p(s_0 = s|\mu, \pi_\theta) := \mu(s)$, and

$$V_\alpha^\pi(s) := \mathbb{E}\left[\sum_{t=0}^{\infty} \gamma^t \left(r(s_t, a_t) - \alpha \log \pi_\theta(a_t|s_t) \right) \middle| s_0 = s \right], \tag{2}$$

is a soft value function. The expectation in eq. (2) is taken under the stochastic trajectory $(s_0, a_0, s_1, \cdots)$ drawn from its distribution $\Pi_{t=0}^{\infty} \pi(a_t|s_t) p(s_t|\mu, \pi_\theta)$.

We use an associated soft Q-function

$$Q_\alpha^\pi(s, a) := r(s, a) + \gamma\, \mathbb{E}_{s'\sim p(\cdot|s,a)} \left[V_\alpha^\pi(s') \right]. \tag{3}$$

The following equation is assumed to hold, for all $s \in \mathcal{S}$, $V_\alpha^\pi(s) = \mathbb{E}_{a\sim\pi(\cdot|s)} \left[Q_\alpha^\pi(s, a) - \alpha \log \pi(a|s) \right]$.

If $\alpha = 0$, eq. (2) is equivalent to an unregularized MDP's objective $\mathbb{E}\left[\sum_{t=0}^{\infty} \gamma^t r(s_t, a_t)\right]$. Hence, in what follows, we do not strictly differentiate between the entropy regularized MDP and the unregularized MDP and for simplicity we just write $V^\pi(s)$ for the value function and $Q^\pi(s, a)$ for the Q-function.

2.2 Model-based Actor-Critic Methods

In this study, we consider a deep model-based actor-critic architecture. Namely, we have neural networks for a policy $\pi_\theta(a|s)$ as an actor, a critic $Q_\phi(s, a)$ approximating $Q^\pi(s, a)$, and a dynamics model $p_\psi(s'|s, a)$ and reward model $r_\psi(s, a)$. The parameters θ, ϕ, and ψ refer to the respective neural network weights.

During critic learning, for an input (s, a), a target signal $\hat{y}$ is computed, and the critic Q_ϕ is updated to minimize the squared difference between its output and $\hat{y}$. Meanwhile, the actor π_θ is updated to maximize the sample average (sampled from a given state distribution) of the estimated value $V^{\pi_\theta}(s) \approx \mathbb{E}_{a\sim\pi_\theta(\cdot|s)} \left[Q_\phi(s, a) - \alpha \log \pi_\theta(a|s) \right]$. Following existing works (Janner et al., 2019; Hafner et al., 2019; Hansen et al., 2022; 2024), we perform alternating updates of the critic and actor within a policy optimization loop. This alternation is explicitly shown in the for loop (line 8) of Algorithm 1.

2.3 Model-Based Policy Optimization (MBPO)

The MBPO algorithm (Janner et al., 2019) applies the policy optimization procedure from SAC (Haarnoja et al., 2018) to fictitious samples generated via model rollouts. Here, we call these rollouts DR. To execute DR, we randomly select initial states from the replay buffer and then simulate D steps using the learned model. The resulting trajectories are stored in a "model buffer", $\mathcal{D}_m^D$, which is separate from the replay buffer.

The critic Q_ϕ is updated to minimize:

$$\mathcal{L}_D(\phi) := \mathbb{E}_{(s,a,r,s')\sim\mathcal{D}_m^D} \left[\left(Q_\phi(s, a) - \hat{y} \right)^2 \right], \tag{4}$$

where the target signal $\hat{y} := r(s,a) + \gamma\, \mathbb{E}_{a'\sim\pi_\theta(\cdot|s')}\big[Q_{\bar{\phi}}(s',a') - \alpha \log \pi_\theta(a'|s')\big]$. Here, $Q_{\bar{\phi}}$ is a target critic with parameters $\bar{\phi}$, which are an exponentially moving average of ϕ (Mnih et al., 2015). $(s,a,r,s') \sim \mathcal{D}_m^D$ and $s \sim \mathcal{D}_m^D$ denote independent sampling operations from the model buffer.

The policy is then updated to maximize

$$\mathcal{J}_D(\theta) := \mathbb{E}_{s\sim\mathcal{D}_m^D}\Big[V_{\phi,\theta}(s)\Big], \tag{5}$$

where

$$V_{\phi,\theta}(s) := \mathbb{E}_{a\sim\pi_\theta(\cdot|s)}\big[Q_\phi(s,a) - \alpha \log \pi_\theta(a|s)\big]. \tag{6}$$

2.4 Training Rollout-based Methods

In this work, we refer to methods that employ the MVE estimator (Feinberg et al., 2018) as *TR-based* with differentiable rollout, a TR. The MVE estimator for a state s uses a T-step TR trajectory $\tau_T = (s_0 = s, a_0, \hat{s}_1, a_1, \cdots, a_{T-1}, \hat{s}_T)$ generated by the policy π_θ and the model p_ψ, to compute:

$$\hat{V}_{\phi,\theta,T}(s) := \sum_{t=0}^{T-1} \gamma^t \left(r_\psi(\hat{s}_t, a_t) - \alpha \log \pi_\theta(a_t|\hat{s}_t)\right) + \gamma^T \hat{V}_\phi(\hat{s}_T), \tag{7}$$

where $\hat{V}_\phi(\hat{s}_T) := Q_\phi(\hat{s}_T, a_T) - \alpha \log \pi_\theta(a_T|\hat{s}_T) \approx \mathbb{E}_{a\sim\pi_\theta(\cdot|\hat{s}_T)}\left[Q_\phi(\hat{s}_T, a) - \alpha \log \pi_\theta(a|\hat{s}_T)\right]$. Even when $\hat{V}_\phi(\hat{s}_T)$ is imperfect due to the critic Q_ϕ struggling to keep pace with a rapidly changing policy, the on-policy reward sequence up to $T-1$ steps improves the overall value estimate at s (Feinberg et al., 2018). Although it is assumed in (Feinberg et al., 2018) that the reward function is known, learning a reward model r_ψ typically poses smaller difficulties than learning a dynamics model or Q-function, so similar benefits are expected.

Following Hafner et al. (2019), we utilize the MVE estimator for learning both of the critic and the policy. Specifically, the critic is trained to approximate the Q-function $Q^{\pi_\theta}(s,a)$ by minimizing

$$\mathcal{L}_Q(\phi) := \mathbb{E}_{(s,a)\sim\mathcal{D}_e}\Big[\big(Q_\phi(s,a) \;-\; \hat{Q}_{\bar{\phi},\theta,T}(s,a)\big)^2\Big], \tag{8}$$

where

$$\hat{Q}_{\bar{\phi},\theta,T}(s,a) := r_\psi(s,a) + \sum_{t=1}^{T-1} \gamma^t \left(r_\psi(\hat{s}_t, a_t) - \alpha \log \pi_\theta(a_t|\hat{s}_t)\right) + \gamma^T \hat{V}_{\bar{\phi}}(\hat{s}_T) \tag{9}$$

For the policy, we maximize

$$\mathcal{J}_T(\theta) := \mathbb{E}_{s\sim\mathcal{D}_e}\Big[\hat{V}_{\phi,\theta,T}(s)\Big]. \tag{10}$$

The gradient $\nabla_\theta \hat{V}_{\phi,\theta,T}(s)$ is computed by combining the reparametrization (RP) trick (Kingma and Welling, 2013) with backpropagation through time. It has been shown that when T becomes large, this process can be prone to gradient explosion (Parmas et al., 2018). Hence, in practice, T is often limited to about 5 steps to maintain stable optimization (Amos et al., 2021).

2.5 Policy-Value Gradient

A key subproblem in policy optimization is to estimate the gradient of the policy parameters, $\nabla_\theta \mathcal{J}(\theta)$, for the objective in (1). We assume the stochastic policy is reparametrized so that for a function $y(a)$: $\mathbb{E}_{a\sim\pi_\theta(a|s)}\left[y(a)\right] = \mathbb{E}_{\epsilon\sim Z}\left[y(\pi_\theta(s,\epsilon))\right]$ where Z is a simple distribution (e.g, Gaussian), and $\pi_\theta(a|s,\epsilon)$ is a deterministic function: $\pi_\theta : (s,\epsilon) \mapsto a$. In this work, we estimate the policy gradient via the RP trick. The policy gradient can be expressed as

$$\nabla_\theta \mathcal{J}\big(\pi_\theta\big) \;=\; \mathbb{E}_{s\sim\mu}\big[\nabla_\theta V^{\pi_\theta}(s))\big] = \mathbb{E}_{s\sim\mu,\varsigma\sim Z}\big[\nabla_\theta Q^{\pi_\theta}(s,\pi(s,\varsigma))\big] \tag{11}$$

$$\;=\; \mathbb{E}_{s\sim\rho^{\pi_\theta},\,\varsigma\sim Z}\Big[\nabla_\theta\, \pi_\theta(s,\varsigma)\;\cdot\; \nabla_a\, Q^{\pi_\theta}(s,a)\big|_{a=\pi_\theta(s,\varsigma)}\Big], \tag{12}$$

as derived in (Zhang et al., 2024), with the last equation derived by extending the deterministic policy gradient theorem (Silver et al., 2014). Here, we assume $\alpha = 0$, and the notation "$\cdot$" denotes an element-wise product summed over the action dimension.

The last term (12) takes only a change of one-step action into account, enabling us to replace Q^{π_θ} with the critic Q_ϕ for the approximation of the partial derivative $\nabla_a Q^{\pi_\theta}(s,a)\big|_{a=\pi_\theta(s,\varsigma)}$. We refer to the estimation $\nabla_\theta \pi_\theta(s,\varsigma) \cdot \nabla_a Q_\phi(s,a)\big|_{a=\pi_\theta(s,\varsigma)}$ as a model-free policy gradient field.

On the other hand, the 1st term is (stochastic) value gradient, of which the term $\nabla_\theta V^{\pi_\theta}(s)$, referred to as a value gradient field, takes into account the change of actions in the future. In an RL setting where the true transition probability is unknown, it is required to use a dynamics model for the estimation. The MVE estimator (7) can be used for the estimation but the terminal term in the gradient with respect to the MVE estimator is a model-free policy gradient field

$$\nabla_\theta \pi_\theta(s,\varsigma) \cdot \nabla_a \hat{V}_\phi(\hat{s}_T)\big|_{a=\pi_\theta(\hat{s}_T,\varsigma)} = \nabla_\theta \pi_\theta(s,\varsigma) \cdot \nabla_a Q_\phi(\hat{s}_T, a_T)\big|_{a_T=\pi_\theta(\hat{s}_T,\varsigma)}$$

Additionally, note that in the last term of (12), the expectation is taken with respect to the discounted state-visitation distribution, whereas in the 1st and 2nd term of (11), it is taken with respect to the initial state distribution. As implied in Zhang et al. (2024), the mixture of initial state distribution and the discounted state-visitation distribution may be preferable, since we have a model-free policy gradient field in the terminal of the value gradient approximated by the MVE estimator.

3 Double Horizon Model-Based Policy Optimization

This section introduces the Double Horizon Model-Based Policy Optimization (DHMBPO) algorithm, which integrates DR and TR to approximate both the state distribution and the value estimation. Before that, we highlight the differences between DR-based methods and TR-based methods.

A procedure common to both DR-based and TR-based methods is to alternate i) sampling states and actions from some distribution $d(s,a)$ and ii) updating policy using samples of estimated policy gradient field.

MBPO samples states and actions from model buffer $\mathcal{D}_m^D$, which is close to an on-policy distribution, and computes model-free policy gradient field:

$$d(s,a) \;=\; \mathcal{D}_m^D \quad \text{and} \quad \nabla_\theta \pi_\theta(s,\varsigma) \cdot \nabla_a Q_\phi(s,a)\big|_{a=\pi_\theta(s,\varsigma)},$$

where, because of DR, sampling from the model buffer can be interpreted as an approximation of ρ^{π_θ} in the term (12).

TR-based methods use a replay buffer $\mathcal{D}_e$ in place of $d(s,a)$ and a value gradient field via the T-step MVE estimator: $\nabla_\theta \hat{V}_{\phi,\theta,T}(s)$:

$$d(s,a) \;=\; \mathcal{D}_e \quad \text{and} \quad \nabla_\theta \hat{V}_{\phi,\theta,T}(s).$$

Note that, as discussed in Section 2.5, sampling from more on-policy distribution is preferable to sampling from the replay buffer.

In DHMBPO, we propose to use a model buffer $\mathcal{D}_m^D$ by DR in place of $\rho_{\pi_\theta}(s)$ and a value gradient field via the T-step MVE estimator:

$$d(s,a) \;=\; \mathcal{D}_m^D \quad \text{and} \quad \nabla_\theta \hat{V}_{\phi,\theta,T}(s),$$

thereby reducing distribution shift by DR without on-policy and real-environment interactions, and improving value estimation by use of MVE estimator via TR.

Concretely, the critic loss function is defined as

$$\mathcal{L}_{D,T}(\phi) := \mathbb{E}_{(s,a)\sim\mathcal{D}_m^D}\Big[\big(Q_\phi(s,a) \;-\; \hat{Q}_{\bar{\phi},\theta,T}(s,a)\big)^2\Big], \tag{13}$$

Algorithm 1 Double Horizon Model-Based Policy Optimization

Require: Models p_ψ and r_ψ, actor network π_θ, critic network Q_ϕ, target critic network $Q_{\bar{\phi}}$, replay buffer $\mathcal{D}_e$, model buffer $\mathcal{D}_m^D$

1: **for** $e = 0, 1, 2, \cdots$ **do**
2: Interact with the environment using π_θ and add observed transitions to $\mathcal{D}_e$
3: Fit the models p_ψ and r_ψ to samples from $\mathcal{D}_e$
4: Sample states from $\mathcal{D}_e$; then perform D-step DR and store the generated transitions in $\mathcal{D}_m^D$
5: **for** $i = 0$ to $L - 1$ **do** ▷ Policy optimization loop
6: Sample states from $\mathcal{D}_m^D$ and execute T-step TR
7: Compute the MVE estimates (7) and (9)
8: Update ϕ to minimize (13) and then update θ to maximize (14) via eq. (11)
9: Clear $\mathcal{D}_m^D$

and the actor's objective is

$$\mathcal{J}_{D,T}(\theta) := \mathbb{E}_{s\sim\mathcal{D}_m^D}\left[\hat{V}_{\phi,\theta,T}(s)\right]. \tag{14}$$

Algorithm 1 presents the procedure for the DHMBPO algorithm. Here L is the length of an episode and repeating policy optimization L times corresponds to a UTD ratio of 1.

Long DR rollouts help maintain on-policy training but increase model bias, thus suggesting an intermediate rollout length for minimizing distribution shift. On the other hand, a longer TR can reduce value estimation error but raise the variance of policy gradients, implying another intermediate horizon for stable gradient estimates. We keep TR in a short-horizon for stable policy gradient estimation and compensate it by using longer DR, toward leveraging model predictions for achieving adequate value estimation accuracy while effective policy improvement. In this work, we set the DR horizon to 20 steps and the TR horizon to 5 steps.

4 Experiments

We validate our DHMBPO on standard continuous control tasks (from Section 4.1 to Section 4.2) and show ablation study in Section 4.3.

4.1 Continuous control benchmark tasks

We evaluate the DHMBPO algorithm on a suite of MuJoCo-based (Todorov et al., 2012) continuous control tasks from Gymnasium (GYM) (Towers et al., 2023) and DMControl (DMC) (Tunyasuvunakool et al., 2020). These tasks range from basic control problems to higher-dimensional robot locomotion, thereby allowing us to investigate the general effectiveness of our approach.

These experiments aim to answer three key questions:

- Does the combined use of DR and TR enhance sample efficiency?
- Does it facilitate efficient critic learning?
- How does DHMBPO compare against other state-of-the-art MBRL algorithms?

All DHMBPO runs share a common set of hyperparameters, which are described along with other implementation details in Appendix A.

Evaluation Protocol. After x environment steps, we measure the algorithm's performance via a *test return*. Specifically, the test return for DHMBPO is based on the sample mean of the cumulative rewards over 10 episodes, whereas some other methods used fewer episodes (See Appendix B for details).

Performance Visualization and Statistical Analysis. We illustrate each method's performance on individual tasks by plotting the mean test return over random seeds (solid line) and its 95% confidence

Table 1: Runtimes (in hours), until 500K environment steps, of DHMBPO, MACURA (Frauenknecht et al., 2024) and SAC-SVG(H) (Amos et al., 2021), on GYM tasks and each ratio to DHMBPO's mean runtime.

Task	DHMBPO	MACURA	SAC-SVG(H)
Ant	3.6	58.3	5.2
HalfCheetah	3.3	32.6	6.7
Hopper	3.7	73.3	6.7
Humanoid	5.2	104.3	6.9
Walker2d	4.0	63.0	6.6
Ratio	1.0	16.8	1.6

interval (shaded area). To aggregate and compare results across multiple tasks, we utilize `rliable` (Agarwal et al., 2021), which offers various statistical tools such as sample efficiency curves and aggregation metrics.

However, because existing works typically focus on either GYM or DMC (but not both), their performance ranges are not directly comparable. We thus apply a task-specific normalization: (i) the number of environment steps is normalized by the maximum step budget for each task, and (ii) the test return is divided by the final performance of a designated baseline. Note that this additional normalization is our adaptation to unify GYM and DMC results. In our GYM comparisons (Figure 2 in Section 4.2), however, we present *raw* (unnormalized) returns to align with common practice (Chua et al., 2018; Janner et al., 2019; Amos et al., 2021; Frauenknecht et al., 2024).

In Section 4.3, we provide an ablation study that isolates the effect of combining DR and TR, and in Section 4.2, we benchmark DHMBPO against several high-performance MBRL algorithms.

4.2 Comparison with State-of-The-Art Algorithms

In this section, we compare the proposed DHMBPO algorithm with several high performance deep MBRL algorithms whose implementations are publicly available.

For the comparison on the GYM suite, we selected five tasks and compared DHMBPO with MBPO (Janner et al., 2019), SAC-SVG(H) (Amos et al., 2021), and MACURA (Frauenknecht et al., 2024). In addition to MBPO, SAC-SVG(H) is an important baseline algorithm, which uses SVG method, a kind of TR-based algorithm. The primary difference between DHMBPO without DR and SAC-SVG(H) is that DHMBPO uses Deep Ensemble models (Lakshminarayanan et al., 2017), whereas SAC-SVG(H) uses a GRU (Cho, 2014) as the deterministic recurrent neural network. Additionally, SAC-SVG(H) learns the critic using one-step TD targets during the TR. MACURA is based on the MBPO algorithm but adaptively adjusts the length of the DR and is reported to achieve state-of-the-art performance on the GYM suite.

For the comparison on DMC suite, we selected 18 tasks and compared DHMBPO with TD-MPC2 (Hansen et al., 2024) and Dreamer v3 (Hafner et al., 2023). Both of these are latent model-based actor-critic algorithms that have demonstrated exceptional performance across multiple benchmark suites, including DMC, using common hyperparameters. TD-MPC2 combines representation learning and reward learning, and during behavior execution, it performs model predictive control (MPC). Dreamer v3 combines representation learning with the MVE estimator from TR, used for training of both the critic and the actor.

4.2.1 Comparison on GYM Tasks

Sample efficiency The results on GYM tasks are shown in Figure 2a, where the sample mean over eight random seeds is plotted as the solid line and 95% credible intervals are shown as the shaded area. For MBPO, five random seeds were used. It is confirmed that DHMBPO achieved the highest sample efficiency across all tasks even without per-task tuning. This large practical performance improvement is perhaps the most important contribution of our work.

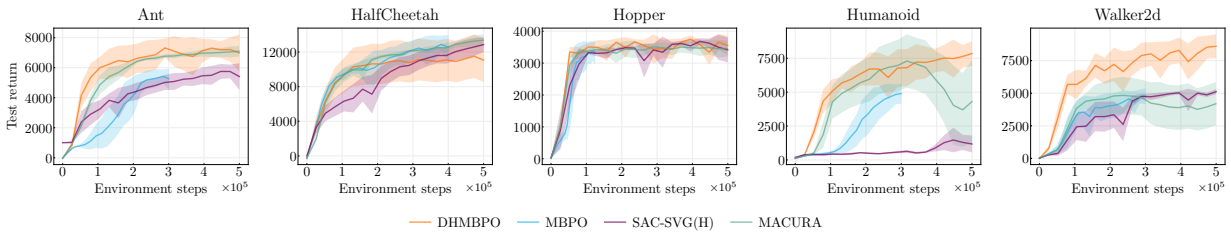

(a) Sample efficiency

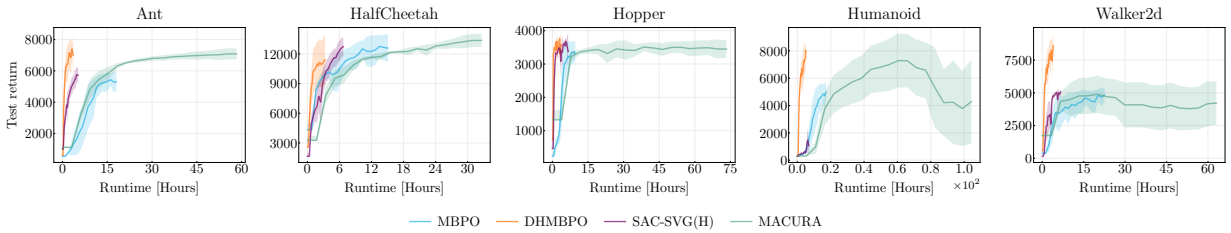

(b) Test return curve as a function of runtime at each constant environment step.

Figure 2: Comparison with state-of-the-art methods on GYM tasks with respect to sample efficiency (upper) and runtime until 500K environment steps (bottom). The solid line represents the sample mean over eight random seeds, and the shaded area indicates the 95% confidence intervals. The runtime plots show that DHMBPO reached the highest test returns the fastest, highlighting the DHMBPO's efficiency with regard to both of sample and runtime cost efficiency.

Runtime Comparison For comparison with respect to runtime for DHMBPO, MACURA, and SAC-SVG(H) on GYM tasks, we show in Figure 2b and summarize it Table 1. Each experiment was executed until 500K environment steps. The computer configuration was NVIDIA RTX A400016GB × 8. Taking into account the aforementioned results on sample efficiency, it can be seen that the DHMBPO algorithm reached 500K steps in less than one-sixteenth of the runtime, while achieving the same or higher degree of sample efficiency as the MACURA. The main reason why MACURA took a relatively long time is its UTD ratio. For example, the UTD ratio for MACURA on `Humanoid` task was 20, while that of DHMBPO (and SAC-SVG(H)) was 1. Although a high UTD ratio promotes higher sample efficiency (Chen et al., 2020; D'Oro et al., 2023), we observed DHMBPO worked well with the UTD ratio of 1, enabling us to save its runtime. Rather, we observed that running at higher UTD ratios did little to increase sample efficiency, while execution time increased (See Figure 20 in Appendix D.5).

4.2.2 Comparison on DMC Tasks

Next, in Figure 3, we present the aggregation metrics on DMC tasks. The metrics are about the test return at 50% normalized steps. The three metrics for each method are shown, where the vertical bars represent the metrics, and the width of the bars corresponds to the 95% confidence intervals. The IQM (Inter Quantile Mean) score shows that DHMBPO exhibited significant performance improvement over the other two methods.

Additional task-specific learning curves and runtime results are provided in Section C.

4.3 Ablation study

Figure 4 shows the experimental results evaluating the sample efficiency of the proposed DHMBPO algorithm and its variants on a set of 10 continuous control benchmark tasks. We selected 5 representative tasks from the GYM suite (upper row) and 5 relatively challenging tasks from the DMC suite (lower row). All compared methods share the same model-learning modules and implementation details, differing only in how the DR and TR are combined.

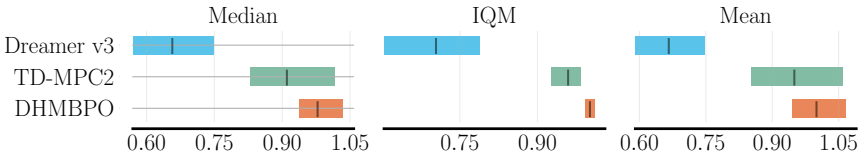

Figure 3: Comparison of aggregation metrics with TD-MPC2 (Hansen et al., 2024) and Dreamer v3 (Hafner et al., 2023) on 18 DMC tasks. The metrics are normalized by DHMBPO's scores. The inter quantile mean (IQM) (Agarwal et al., 2021) score shows significant improvement, demonstrating DHMBPO's advantage over the other methods.

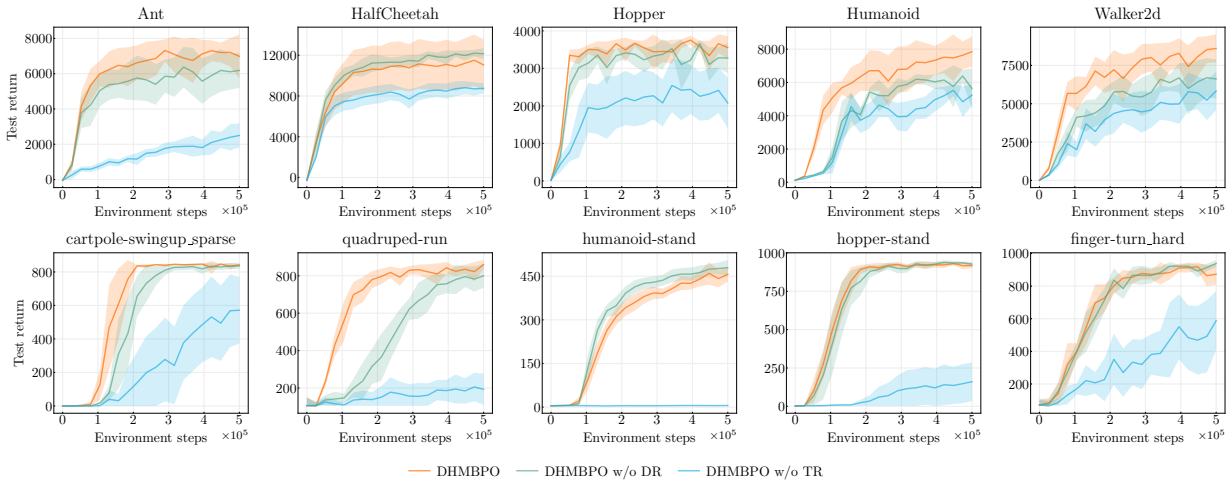

Figure 4: Performance comparison of DHMBPO (orange) against its two ablated variants: DHMBPO without DR (w/o DR, corresponding to SAC-SVG(H), green) and DHMBPO without TR (w/o TR, corresponding to MBPO, blue). The top row shows results on five representative tasks from the GYM suite, and the bottom row shows results on five more challenging tasks from the DMC suite. Each solid line represents the mean test return over 8 random seeds, and the shaded regions denote the 95% confidence intervals. The proposed DHMBPO configuration (DR horizon = 20, TR horizon = 5) consistently outperforms both variants.

We consider three configurations of DHMBPO corresponding to different (DR horizon, TR horizon) settings: **DHBMPO (20, 5)**, the proposed algorithm, uses both DR and TR. **DHMBPO without DR (0, 5)**: samples initial states from replay buffer and uses them for TR. This setup corresponds to SAC-SVG(H). **DHMBPO without TR (20, 0)** samples initial states from model buffer and applies the policy optimization procedure in SAC, as described in Section 2.3. This setup corresponds to MBPO.

For each configuration, we ran experiments with 8 different random seeds. The solid lines in Figure 4 represent the mean performance across these seeds, while the shaded areas indicate the 95% confidence intervals.

The results show that combining DR and TR outperforms using either DR or TR alone. In particular, the DHMBPO configuration (20, 5) achieves higher returns and better sample efficiency compared to the two reduced versions. For example, the TR-only variant (0, 5) corresponds to SAC-SVG(H); while it benefits from improved value estimation, the absence of DR leads to reliance on off-policy samples, resulting in less sample efficiency in challenging tasks like `Humanoid`, `Walker2d`, and `quadruped-run`. Meanwhile, the DR-only variant (20, 0) corresponds to MBPO; although it can approximate the on-policy state distribution, the lack of TR's MVE estimation fails to provide effective value corrections, leading to notably inferior performance on all tasks. Overall, these results demonstrate that the synergy achieved by combining DR and TR in DHMBPO leads to faster learning than either technique alone.

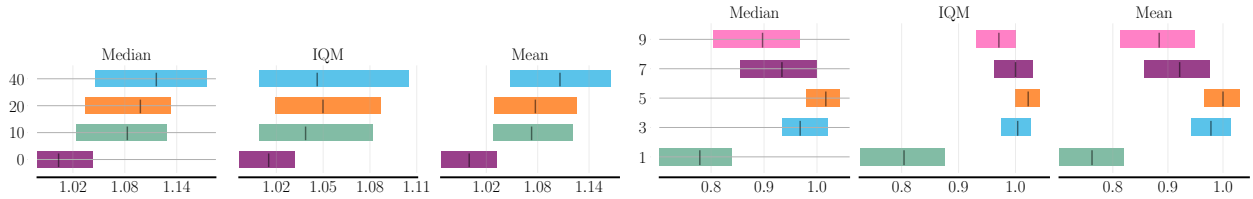

(a) Variants of DR horizon.

(b) Variants of TR horizon.

Figure 5: Aggregation metrics on 10 tasks for (a) variants of different DR horizons and (b) variants of different TR horizons.

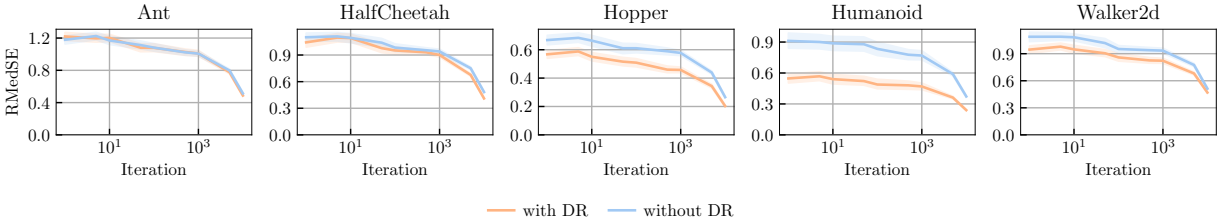

Figure 6: Development of the RMedSE for DHMBPO (Orange) and DHMBPO without DR (Blue). The x-axis is the number of iterations for an update of the critic parameter while all other models are fixed. y-axis is the normalized RMedSE about Monte Carlo return (N=256) from the target environment.

We include additional experiments, in Appendix D.1, for DHMBPO without TR, corresponding to MBPO, but with different UTD ratios. Increasing the UTD ratio improved sample efficiency (Figure 11) but also led to longer execution times (Figure 12). In other words, achieving high sample efficiency without TR requires sacrificing computation cost by raising the UTD ratio. On the other hand, DHMBPO achieved high sample efficiency without increasing the UTD ratio (Figure 4), indicating that introducing TR helps reduce computational cost. Indeed, as shown in Section 4.2, DHMBPO attained a sample efficiency comparable to state-of-the-art MBPO-based methods in a shorter execution time.

4.4 Hyper-parameter sensitivity

Figure 5 illustrates our sensitivity analysis of the distribution-rollout (DR) and training-rollout (TR) horizon hyperparameters. We evaluated 10 tasks under 8 random seeds, measuring test return after 500K environment steps. To avoid bias toward any single metric, the figure reports three summary statistics—median, inter-quantile mean (IQM), and mean—along with 95% confidence intervals.

We chose DR=20 and TR=5 as our baseline. In Figure 5a, we varied only the DR horizon (0, 10, 20, 40), while keeping TR=5 fixed. In Figure 5b, we varied only the TR horizon (1, 3, 5, 7, 9), while keeping DR=20 fixed. The results show that: 1). DR benefits from being relatively long (e.g., 20) compared to short horizons (e.g., 0). 2). TR=5 offers a good balance between sample efficiency and gradient stability. Short TR reduces sample efficiency (similar to "DHMBPO w/o TR" in Figure 4), while too long TR can cause gradient norms to explode (see Appendix C.3, Figure 10b), destabilizing learning. Furthermore, in Section D.2, we provide the investigation of trade-off in policy gradient through TR and a practical way to determine a better TR horizon based on a small number of real samples.

Overall, these findings suggest setting DR to a moderately long horizon and TR to a shorter, carefully chosen horizon to prevent gradient explosion and maintain robust performance.

4.5 Efficient Critic Learning

We show the benefit of DR in critic learning, a more accurate value estimation. We ran DHMBPO for 100K environment steps on five environments from the GYM suite. After this training, the learned dynamics model and actor network were fixed. We then re-initialized critic networks and compared two variants for critic learning: **with DR:** Use model-generated rollouts (stored in a model buffer) to train the critic. **without DR:** Use only samples from the replay buffer, without additional model-based rollouts.

As ground truth values, we computed a Monte Carlo return $\hat{Q}_g(s,a)$ from 2,048 rollouts in the real environment, for each of 256 randomly sampled state-action pairs (s,a) taken from the replay buffer. We then calculated MVE estimate $\hat{Q}_{\bar{\phi},\theta,5}(s,a)$ for the 256 state-action pairs, and measured its discrepancy from $\hat{Q}_g(s,a)$ via a normalized root median squared error (RMedSE):

$$E(i) \;:=\; \sqrt{\text{Median}\left[\left(\frac{\hat{Q}_g(s,a) - \hat{Q}_{\bar{\phi},\theta,5}(s,a)}{\hat{Q}_g(s,a)}\right)^2\right]},$$

where i is the critic optimization step. "Median" denotes the median over the selected 256 state-action pairs. For each setup, we repeated the procedure with 32 different random seeds for the critic's initialization and plotted the mean (solid line) and the 95% confidence intervals (shaded area) of $E(i)$ as a function of i.

As in the environment of the last three panels in Figure 6, we observe that *with DR* exhibits a significantly lower estimation error, particularly at the early stages of training. This difference indicates that the MVE estimator is more accurately approximating the true value function. Since the policy is continuously updated throughout training, an early advantage in value estimation can accumulate and benefit each subsequent optimization step. In the `Humanoid` environment specifically, we believe this improved value estimation under DR leads to the notable gains in sample efficiency shown in Figure 4.

5 Related Work

Many practical off-policy actor-critic methods, including the SVG algorithm, rely on uniform sampling from the replay buffer. While importance sampling corrections have been proposed in model-free reinforcement learning (Hallak and Mannor, 2017; Zhang et al., 2020), they are prone to issues such as high variance in the likelihood ratios (Liu et al., 2019).

In MBRL, MBPO (Janner et al., 2019) introduced DR, achieving high sample efficiency. However, MBPO suffers from the issue of requiring extensive runtime. In contrast, while MBPO uses the model solely for generating virtual data, the SVG method is expected to leverage the differentiability of the model directly in the optimization of the policy, enabling more efficient learning.

PILCO (Deisenroth and Rasmussen, 2011), which employs Gaussian processes (GPs) as a model, demonstrates very high sample efficiency by performing policy optimization using SVG on the analytical distribution of the cumulative reward. However, when using sample-based predictions instead of assuming an analytical distribution, the gradient estimation becomes unstable, especially for long prediction horizons, as errors accumulate over time (Parmas et al., 2018). This issue is particularly pronounced in tasks where accurate long-term predictions are crucial.

Furthermore, as discussed in Section 3, SVG methods have not adequately addressed the problem of distribution shift in the objective function. Specifically, Feinberg et al. (2018) explored the usefulness of model-based value estimation and derived conditions for an on-policy stationary distribution, but the utility of combining these conditions with SVG for policy optimization was not made clear. In this study, we introduce a novel approach that uses the MVE estimator for both actor and critic learning, resolving the distribution shift issue. This constitutes the key novelty of our work.

Finally, while it is possible to consider using IS to resolve the distribution shift as in model-free reinforcement learning literature, our study focuses on achieving practical performance improvements. We demonstrate that simply adding the DR leads to performance gains without a large runtime increase. This simple yet

effective approach proves to be highly beneficial in developing technologies for RL problems where sample efficiency is important.

6 Conclusion

In this study, we introduced DHMBPO, a new MBRL algorithm that integrates two separate model rollouts —a long-horizon DR and a short-horizon TR— to tackle two aspects of the trade-off: (i) state distribution shift versus model bias, and (ii) accuracy in value and value gradient versus policy gradient instability. Long DR resamples from the model to better approximate the on-policy state distribution, whereas short TR leverages differentiable transitions to offer accurate on-policy value estimation with stable gradient updates, thereby requiring fewer updates and reducing overall runtime. By assigning different horizon lengths to DR and TR, we preserve sample efficiency without incurring excessive model-bias and increased runtime.

Experimental results on multiple continuous-control tasks indicate that DHMBPO consistently achieves faster learning and short runtime compared to existing MBRL baselines. We observe that the synergy of a long DR with a short TR enables early improvements in value estimation, which accumulate over successive policy updates. Although the method provides a more balanced solution to the model-bias versus off-policy-data challenge, exploration remains an open issue. For instance, certain tasks such as `finger-spin` (Figure 8 in Appendix C), can still lead to local optima. Nonetheless, the relatively short runtime of DHMBPO facilitates iterative refinement and experimentation, thereby offering a cost-effective path toward practical performance gains in development of reinforcement learning applications where the sampling cost is critical.

References

Rishabh Agarwal, Max Schwarzer, Pablo Samuel Castro, Aaron C Courville, and Marc Bellemare. Deep reinforcement learning at the edge of the statistical precipice. *Advances in Neural Information Processing Systems*, 34, 2021. 4.1, 3

Brandon Amos, Samuel Stanton, Denis Yarats, and Andrew Gordon Wilson. On the model-based stochastic value gradient for continuous reinforcement learning. In *Learning for Dynamics and Control*, pages 6–20. PMLR, 2021. 1, 2.4, 1, 4.1, 4.2, B, D.3

Jimmy Lei Ba, Jamie Ryan Kiros, and Geoffrey E Hinton. Layer normalization. *arXiv preprint arXiv:1607.06450*, 2016. A.1.1

G Brockman. Openai gym. *arXiv preprint arXiv:1606.01540*, 2016. 1

Jacob Buckman, Danijar Hafner, George Tucker, Eugene Brevdo, and Honglak Lee. Sample-efficient reinforcement learning with stochastic ensemble value expansion. *Advances in neural information processing systems*, 31, 2018. A.5

Xinyue Chen, Che Wang, Zijian Zhou, and Keith W Ross. Randomized Ensembled Double Q-Learning: Learning Fast Without a Model. In *International Conference on Learning Representations*, 2020. 4.2.1, A.1.2

Kyunghyun Cho. Learning phrase representations using RNN encoder-decoder for statistical machine translation. *arXiv preprint arXiv:1406.1078*, 2014. 4.2, D.3

Kurtland Chua, Roberto Calandra, Rowan McAllister, and Sergey Levine. Deep Reinforcement Learning in a Handful of Trials using Probabilistic Dynamics Models. *Adv. Neural Inf. Process. Syst.*, 2018-Decem (Nips):4754–4765, 2018. 4.1, A.2

Marc Deisenroth and Carl E Rasmussen. PILCO: A model-based and data-efficient approach to policy search. In *Proceedings of the 28th International Conference on machine learning (ICML-11)*, pages 465–472, 2011. 1, 5

Pierluca D'Oro, Max Schwarzer, Evgenii Nikishin, Pierre-Luc Bacon, Marc G Bellemare, and Aaron Courville. Sample-Efficient Reinforcement Learning by Breaking the Replay Ratio Barrier. In *The Eleventh International Conference on Learning Representations*, 2023. URL https://openreview.net/forum?id=OpC-9aBBVJe. 4.2.1

Stefan Elfwing, Eiji Uchibe, and Kenji Doya. Sigmoid-weighted linear units for neural network function approximation in reinforcement learning. *Neural networks*, 107:3–11, 2018. A.1.1

Vladimir Feinberg, Alvin Wan, Ion Stoica, Michael I Jordan, Joseph E Gonzalez, and Sergey Levine. Model-based value expansion for efficient model-free reinforcement learning. In *Proceedings of the 35th International Conference on Machine Learning (ICML 2018)*, 2018. 1, 2.4, 2.4, 5

Bernd Frauenknecht, Artur Eisele, Devdutt Subhasish, Friedrich Solowjow, and Sebastian Trimpe. Trust the model Where it trusts itself – model-Based Actor-Critic with uncertainty-Aware Rollout Adaption. *arXiv [cs.LG]*, 2024. 1, 4.1, 4.2, B

Matthieu Geist, Bruno Scherrer, and Olivier Pietquin. A theory of regularized markov decision processes. In *International Conference on Machine Learning*, pages 2160–2169. PMLR, 2019. 2.1

Tuomas Haarnoja, Aurick Zhou, Pieter Abbeel, and Sergey Levine. Soft actor-critic: Off-policy maximum entropy deep reinforcement learning with a stochastic actor. In *International Conference on Machine Learning*, pages 1861–1870. PMLR, 2018. 2.3

Danijar Hafner, Timothy Lillicrap, Jimmy Ba, and Mohammad Norouzi. Dream to Control: Learning Behaviors by Latent Imagination. 2019. 1, 2.2, 2.4

Danijar Hafner, Jurgis Pasukonis, Jimmy Ba, and Timothy Lillicrap. Mastering diverse domains through world models. *arXiv preprint arXiv:2301.04104*, 2023. 4.2, 3, B

Assaf Hallak and Shie Mannor. Consistent on-line off-policy evaluation. In *International Conference on Machine Learning*, pages 1372–1383. PMLR, 2017. 1, 5

Nicklas Hansen, Hao Su, and Xiaolong Wang. TD-MPC2: Scalable, Robust World Models for Continuous Control. In *The Twelfth International Conference on Learning Representations*, 2024. 1, 2.2, 4.2, 3, B

Nicklas A Hansen, Hao Su, and Xiaolong Wang. Temporal Difference Learning for Model Predictive Control. In *International Conference on Machine Learning*, pages 8387–8406. PMLR, 2022. 2.2

Nicolas Heess, Gregory Wayne, David Silver, Timothy Lillicrap, Tom Erez, and Yuval Tassa. Learning continuous control policies by stochastic value gradients. *Advances in neural information processing systems*, 28, 2015. 1

Takuya Hiraoka, Takahisa Imagawa, Taisei Hashimoto, Takashi Onishi, and Yoshimasa Tsuruoka. Dropout q-functions for doubly efficient reinforcement learning. In *International Conference on Learning Representations*, 2022. 1, 1

Michael Janner, Justin Fu, Marvin Zhang, and Sergey Levine. When to Trust Your Model: Model-Based Policy Optimization. In *Advances in Neural Information Processing Systems*, volume 32. Curran Associates, Inc., 2019. 1, 2.2, 2.3, 4.1, 4.2, 5, A.1.1, B

Diederik P Kingma and Max Welling. Auto-encoding variational bayes. *arXiv preprint arXiv:1312.6114*, 2013. 1, 2.4

Balaji Lakshminarayanan, Alexander Pritzel, and Charles Blundell. Simple and scalable predictive uncertainty estimation using deep ensembles. *Advances in neural information processing systems*, 30, 2017. 4.2

Yao Liu, Adith Swaminathan, Alekh Agarwal, and Emma Brunskill. Off-policy policy gradient with state distribution correction. *arXiv preprint arXiv:1904.08473*, 2019. 1, 5

Ilya Loshchilov and Frank Hutter. Decoupled Weight Decay Regularization. In *International Conference on Learning Representations*, 2019. 2

Volodymyr Mnih, Koray Kavukcuoglu, David Silver, Andrei A Rusu, Joel Veness, Marc G Bellemare, Alex Graves, Martin Riedmiller, Andreas K Fidjeland, Georg Ostrovski, et al. Human-level control through deep reinforcement learning. *Nature*, 518(7540):529–533, 2015. 2.3

Paavo Parmas, Carl Edward Rasmussen, Jan Peters, and Kenji Doya. PIPPS: Flexible model-based policy search robust to the curse of chaos. In *International Conference on Machine Learning*, pages 4065–4074. PMLR, 2018. 1, 2.4, 5

Luis Pineda, Brandon Amos, Amy Zhang, Nathan O. Lambert, and Roberto Calandra. MBRL-Lib: A Modular Library for Model-based Reinforcement Learning. *Arxiv*, 2021. B, D.4

David Silver, Guy Lever, Nicolas Heess, Thomas Degris, Daan Wierstra, and Martin Riedmiller. Deterministic policy gradient algorithms. In Eric P Xing and Tony Jebara, editors, *Proceedings of the 31st International Conference on Machine Learning*, volume 32 of *Proceedings of Machine Learning Research*, pages 387–395, Bejing, China, 2014. PMLR. 1, 2.5

Nitish Srivastava, Geoffrey Hinton, Alex Krizhevsky, Ilya Sutskever, and Ruslan Salakhutdinov. Dropout: a simple way to prevent neural networks from overfitting. *The journal of machine learning research*, 15(1): 1929–1958, 2014. A.1.1

Richard S Sutton, David McAllester, Satinder Singh, and Yishay Mansour. Policy gradient methods for reinforcement learning with function approximation. *Advances in neural information processing systems*, 12, 1999. 1

Emanuel Todorov, Tom Erez, and Yuval Tassa. Mujoco: A physics engine for model-based control. In *2012 IEEE/RSJ international conference on intelligent robots and systems*, pages 5026–5033. IEEE, 2012. 4.1

Mark Towers, Jordan K. Terry, Ariel Kwiatkowski, John U. Balis, Gianluca de Cola, Tristan Deleu, Manuel Goulão, Andreas Kallinteris, Arjun KG, Markus Krimmel, Rodrigo Perez-Vicente, Andrea Pierré, Sander Schulhoff, Jun Jet Tai, Andrew Tan Jin Shen, and Omar G. Younis. Gymnasium, 2023. URL https://zenodo.org/record/8127025. 4.1

Saran Tunyasuvunakool, Alistair Muldal, Yotam Doron, Siqi Liu, Steven Bohez, Josh Merel, Tom Erez, Timothy Lillicrap, Nicolas Heess, and Yuval Tassa. dm_control: Software and tasks for continuous control. *Software Impacts*, 6:100022, 2020. 4.1

Shangtong Zhang, Bo Liu, Hengshuai Yao, and Shimon Whiteson. Provably convergent two-timescale off-policy actor-critic with function approximation. In *International Conference on Machine Learning*, pages 11204–11213. PMLR, 2020. 5

Shenao Zhang, Boyi Liu, Zhaoran Wang, and Tuo Zhao. Model-based reparameterization policy gradient methods: Theory and practical algorithms. *Advances in Neural Information Processing Systems*, 36, 2024. 1, 2.5

A Implementation Detail

Neural network architectures for dynamics and reward model, actor and critics is explained in Section A.1. About the dynamics and reward model, we describe how to predict the model in Section A.2 and how to train it in Section A.3. Hyperparameters are listed in Section A.4. Finally we describe technique for stable critic's prediction in Section A.5.

A.1 Neural network models

A.1.1 Dynamics and reward model

Following Janner et al. (2019), we employ a bootstrap ensemble of $M = 8$ models,

$$\{p_{\psi_1}, p_{\psi_2}, \cdots, p_{\psi_M}\}.$$

We refer to them as deep ensemble (DE) models. As discussed in Section A.3, each ensemble member is trained on (virtually) independent bootstrapped datasets. The ensemble members model aleatoric noise by fitting independent multivariate Gaussian distributions.

Concretely, the m-th model $p_{\psi_m}(s, a)$ takes a state-action pair $x = (s, a)$ as input and outputs the mean vector $\mu_m \in \mathbb{R}^{S+1}$ of a multivariate Gaussian distribution. Here, S is the dimension of the continuous state space, and we jointly predict the next state (S dimensions) plus the reward (1 dimension), hence the total output dimension $S + 1$. For the covariance, we assume homoscedastic noise, meaning that each model's diagonal covariance elements $\sigma_m^2 \in \mathbb{R}^{S+1}$ are constant with respect to the input.

We use Layer normalization (Ba et al., 2016) and Dropout (Srivastava et al., 2014) for regularization, and apply SiLU (Elfwing et al., 2018) as the activation function.

Below is a PyTorch-like summary of our network architecture:

```
(model): Sequential(
    (0): EnsembleLinearLayer(
        8, in_size=S+A, out_size=256, decay=0.00025)
    (1): Dropout(p=0.0075)
    (2): SiLU()
    (3): LayerNorm((256,))
    (4): EnsembleLinearLayer(
         8, in_size=256, out_size=256, decay=0.0005)
    (5): Dropout(p=0.005)
    (6): SiLU()
    (7): LayerNorm((256,))
    (8): EnsembleLinearLayer(
         8, in_size=256, out_size=256, decay=0.00075)
    (9): Dropout(p=0.0025)
    (10): SiLU()
    (11): LayerNorm((256,))
    (12): EnsembleLinearLayer(
         8, in_size=256, out_size=S+1, decay=0.001)
  )
)
```

"EnsembleLinearLayer" denotes the layer which calculates the feed forward pass in parallel.

A.1.2 Actor and Critics

We also use ensemble of MLP as critic networks used for randomized ensemble double Q-learning, or RED-Q (Chen et al., 2020). We summarize the neural network architecture using Pytorch-like notation:

for model,

```
(critics): Sequential(
    (0): EnsembleLinearLayer(
        5, in_size=S+A, out_size=512, decay=0.0)
    (1) Dropout(p=0.0001)
    (2): SiLU()
    (3) LayerNorm((256,))
    (4): EnsembleLinearLayer(
        5, in_size=512, out_size=512, decay=0.0)
    (5) Dropout(p=0.0001)
    (6): SiLU()
    (7) LayerNorm((256,))
    (8): EnsembleLinearLayer(
        5, in_size=512, out_size=512, decay=0.0)
    (9) Dropout(p=0.0001)
    (10): SiLU()
    (11) LayerNorm((256,))
    (12): EnsembleLinearLayer(
        5, in_size=512, out_size=1, decay=0.0)
  )
)
```

for critic networks, and

```
(actor): Sequential(
    (0): Linear(in_features=S, out_features=512)
    (1): SiLU()
    (2): Linear(in_features=512, out_features=512)
    (3): SiLU()
    (4): Linear(in_features=512, out_features=512)
    (5): SiLU()
    (6): Linear(in_features=512, out_features=2A)
  )
)
```

for actor networks, respectively, where S is the dimension of state space, and A is the dimension of action space. The total number of weight parameters, for example on `Humanoid` task from GYM suite is about 2M, where S=45 and A=17.

A.2 Model prediction

We propose to normalize the signals targeted for regression (See Section A.3 for more detail). Given a variable z, we denote its normalized version by $\bar{z}$. We perform normalization by the empirical mean μ_z and standard deviation σ_z statistics of the variable with the equation $\bar{z} := \frac{z-\mu_z}{\sigma_z}$. Similarly, we can perform denormalization by $z = \bar{z}\sigma_z + \mu_z$. We denote the state vectors and the next-state vectors as $s, s' \in \mathbf{R}^{d_S}$ respectively, and the i-th element of the displacement between them as $\Delta_i := {s'}_i - s_i$. Our dynamics models, T_ψ, are trained to predict the displacements in states from one step to the next, thus we normalize the outputs based on their used targets. Let μ_{Δ_i} and σ_{Δ_i} be the mean and standard deviation of the observed displacements in the data up to now. During training the model, the i-th element of the model's target signal for the n-th data point is defined as $\bar{t}_{ni} := \frac{\Delta_{ni}-\mu_{\Delta_i}}{\sigma_{\Delta_i}}$. We summarize the different normalizations we perform: all inputs to models are normalized; the rewards are normalized during training the reward model, but the predicted rewards are denormalized during policy learning; the actions are never normalized (as we choose their scale to be reasonable); the transition model targets are normalized during model training and also during the actor training rollouts.

The rollout predictions, in particular, require care in the implementation. Suppose the normalized state is $\bar{s}$ and the transition model has predicted a change $\bar{\Delta}$. We can add the normalized displacement to the normalized state by first denormalizing, then adding them, then normalizing them again. This leads to the process: (i) $s = \mu_s + \sigma_s\bar{s}$, (ii) $\Delta = \mu_\Delta + \sigma_\Delta\bar{\Delta}$, (iii) $s' = s + \Delta = \mu_s + \sigma_s\bar{s} + \mu_\Delta + \sigma_\Delta\bar{\Delta}$, (iv) $\bar{s}' = \frac{s'-\mu_s}{\sigma_s} = \bar{s} + \frac{\mu_\Delta+\sigma_\Delta\bar{\Delta}}{\sigma_s}$. We thus see that to make correct predictions in the normalized space using our displacement model, we need to denormalize the displacements, then normalize them using the normalization scale of the states, s, and add the displacement to the normalized state, $\bar{s}$.

Note that although a similar normalization was performed in SAC-SVG(H), the output was normalized using the sample mean and standard deviation of the state, just like the input.

When predicting next-state and reward during rollout, we adopt the TS-1 algorithm proposed in Chua et al. (2018), which randomly selects an ensemble member for each input and timestep in order to propagate uncertainty through bootstrapping.

A.3 Model Learning

A.3.1 The objective function

The objective of the model learning is minimizing the sum of the negative log-likelihood:

$$\mathcal{L}(\psi) := \frac{1}{MND}\sum_{m=1}^{M}\sum_{n=1}^{N} w_{mn}\mathcal{L}_{mn}$$

where

$$\mathcal{L}_{mn} := \sum_{d=1}^{D}\left\{\log\sigma_{md} + \frac{1}{2}\left(\frac{\bar{t}_{nd}-\mu_{mnd}}{\sigma_{md}}\right)^2\right\}.$$

$\mu_{mnd} := \mu^{(d)}_{\psi_m}(x_n)$ represents the dth output of the mth neural network μ_{ψ_m} for the nth input $x_n := (s_n, a_n)$, and σ_{md} denotes the noise regarding the dth dimension output of the mth ensemble member σ_m.

$w_{mn} \in [0, \infty]$ is a weight for nth sample allocated to the mth model, in order to make the dataset virtually independent bootstrapped one. The value is randomly sampled from the exponential distribution $f(w|1)$ with the parameter $\lambda = 1$ and fixed, thus the effective number of data used for each model's learning is equivalent on average.

A.3.2 Early stopping

When x_n is the input, let μ_{mn} and σ_m represent the mean and scale parameter, of the mth model's predicted Gaussian distribution. We aggregate the predictions across all ensemble members, and define the prediction of the DE models as a Gaussian distribution with mean parameters for the dth dimension when the input is x_n as $\tilde{\mu}_{nd} := \frac{1}{M}\sum_{m=1}^{M}\mu_{mnd}$ and the scale parameter as $\tilde{\sigma}^2_{nd} := s^2_{nd} + \frac{1}{M}\sum_{m=1}^{M}\sigma^2_{md}$, where s^2_{nd} is the sample variance among the ensemble of predictions $\{\mu_{mnd}\}_{m=1}^{M}$. This approach is often also called moment matching.

Then, we define the evaluation score S_n for the nth data as:

$$S_n := \frac{1}{2}\sum_{d=1}^{D}\left[\frac{(\tilde{\mu}_{nd} - t_{nd})^2}{\tilde{\sigma}^2_{nd}} + \log \tilde{\sigma}^2_{nd}\right]$$

under the assumption that the predicted distribution follows a Gaussian distribution with a diagonal covariance matrix. After each epoch of model learning, we evaluate the score for each validation data point and compare the distribution of these scores based on the new parameters of the model with those from the previous parameters. If the distribution of the new scores shows significant improvement according to a Z-test with a significance level of 0.1, we continue training the model.

Our stopping strategy is the same as in the MBPO implementation: if the new model does not show improvement over a fixed number of epochs, the training is stopped. We set the threshold as $b \log d_s$, where b is a scalar-valued hyper-parameter, representing the base number of epochs, and d_s is the dimension of the state space.

A.4 Hyper-parameters

We summarize in Table 2 hyper-parameters shared for all experiments in Section 4.

A.5 Bounding target critic's output

In this study, we use the MVE estimator for Q-function, eq. (9) as the target values in critic learning. However, due to the recursive dynamics model predictions, the model errors may accumulate or value estimation errors may increase (Buckman et al., 2018). In order to avoid this risk, we bound the values predicted by the target critics to stabilize critic learning.

Since the Q-value is within $\frac{1}{1-\gamma}$ times the upper and lower bounds of the reward value (*Proof.* $\sum_{h=0}^{\infty}\gamma^h r_h \leq \sum_{h=0}^{\infty}\gamma^h r_{\max} = \frac{1}{1-\gamma}r_{\max}$ and similar for the lower bound), we approximate these upper and lower reward bounds. The procedure for estimation of bounds on Q^{π_θ} is as follows: (1) Perform training rollouts. (2) Set the 1-st and 99-th percentiles of rewards from the rollouts as r_l and r_u, respectively. (3) $Q_l := \frac{r_l}{1-\gamma}$ and $Q_u := \frac{r_u}{1-\gamma}$. (4) When calculating the bounds for the first time, set Q_l and Q_u as the initial values, and subsequently update them by taking exponential moving averages with a hyperparameter η. Then we clip the target critic networks' outputs in eq. (9) by Q_l and Q_u. Since the process is simple, its computation cost is negligible.

We do not perform, on the other hand, clipping on the output of the critic used when training actor with eq. (7). This is because if the critic network outputs a value outside the bounds, the gradient to encourage predicting values within that range would vanish because of the clipping.

Table 2: Hyper-parameters for DHMBPO used across all experiments in this study

Hyper-parameter	Value
Discount factor	0.995
Seed steps	5000
Action repeat	1 (Gym) 2 (DMControl)
Batch size	256
Update-to-data ratio	1
Replay buffer size	1M
Learning rate for the actor, critics and α	$3 \cdot 10^{-4}$
Initial value of α	0.1
Momentum coefficient c for target critic	0.995
Length of DR D	20
Length of training rollout T	5
Iteration per DR	20
Ensemble size of model	8
Optimizer for training model	AdamW (Loshchilov and Hutter, 2019)
Learning rate training model	$1 \cdot 10^{-3}$

The motivation for using percentiles in the step (2), instead of using a hard max and min, is based on the observation in our preliminary experiments (Appendix D.6). There are occasional large outliers in the rewards that would make the bounds extremely broad. Ignoring these outliers, but estimating the bounds based on the most of the samples gives more efficient and stable results.

B Experiment Details

We describe configuration for comparison in Section 4.2. In this study, when the other algorithms' experimental results under identical settings were available, we used those results as part of the results (MBPO and Dreamer v3). For the rest of the results, we ran the publicly available source code with its default hyperparameter settings.

The number of samples to measure a test return varies depending on the implementation of the algorithm. Like DHMBPO, SAC-SVG(H) (Amos et al., 2021) and TD-MPC2 (Hansen et al., 2024) used 10 test episodes, while as MACURA (Frauenknecht et al., 2024) used 3 test episodes and MBPO (Janner et al., 2019; Pineda et al., 2021) and Dreamer v3 (Hafner et al., 2023) used 1 test episode.

For each GYM tasks, except for DHMBPO, each algorithms' hyper-parameters were tuned per-task. Following (Janner et al., 2019), we used variants for the `Humanoid` and `Ant` environments from GYM, with some state dimensions truncated to lower dimensions.

For DMC tasks, Each of three algorithms' hyper-parameters were set commonly over all DMC tasks.

C Result Details

C.1 Ablation study

Figure 7 shows performance profile and score distributions of ablated algorithms on 5 GYM tasks and 5 DMC tasks, of which individual plots are shown in Section 4.3. We see that DHMBPO's statistically significant sample efficiency in early phase against the ablated algorithms.

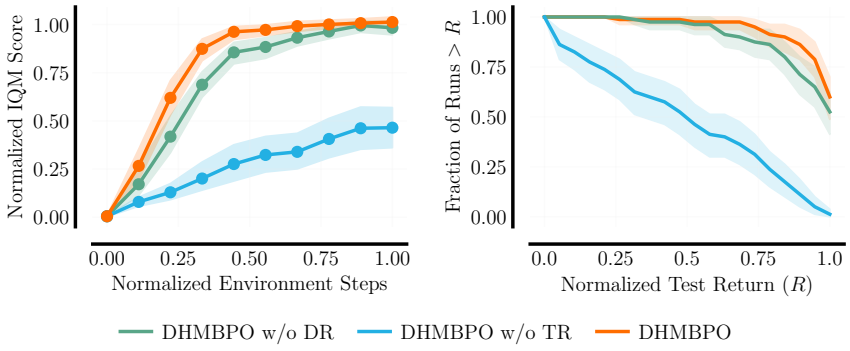

Figure 7: Performance profile (*left*) and score distributions (*right*) of ablated algorithms on 5 GYM tasks and 5 DMC tasks.

Table 3: Runtimes on DMC tasks until maximum environment step budget (250K or 500K) and its ratio to DHMBPO's mean runtime (in hours).

	DHMBPO	Dreamer v3	TD-MPC2
acrobot-swingup	1.7	2.9	3.8
acrobot-swingup_sparse	1.6	2.9	2.6
cartpole-balance	0.9	1.5	1.2
cartpole-swingup	0.9	2.9	1.9
cartpole-swingup_sparse	1.9	2.9	2.3
cheetah-run	2.7	4.1	2.8
cup-catch	1.2	1.6	1.9
finger-spin	2.2	3.2	2.9
finger-turn_easy	2.2	3.2	2.7
finger-turn_hard	2.2	3.2	2.6
hopper-hop	2.7	3.1	3.8
hopper-stand	3.2	3.3	2.3
humanoid-stand	4.3	2.9	5.0
quadruped-run	3.7	3.2	2.7
reacher-hard	2.0	2.9	3.7
walker-run	2.7	3.2	3.9
walker-stand	1.2	1.6	1.8
walker-walk	1.7	1.5	3.7
Ratio	1.0	1.3	1.3

C.2 Comparison with other algorithms

For DMC tasks, we provide plots for individual sample efficiency curve in Figure 8, plots for runtime in Figure 9 and Table 3 for summarizing their runtimes.

C.3 Hyper-parameter sensitivity

We show individual results of experiments in Section 4.4 with respect to sample efficiency (a) and to an Euclidean norm of policy gradient $\theta \in \mathcal{R}^D$: $\sqrt{\sum_i^D \theta_i^2}$.

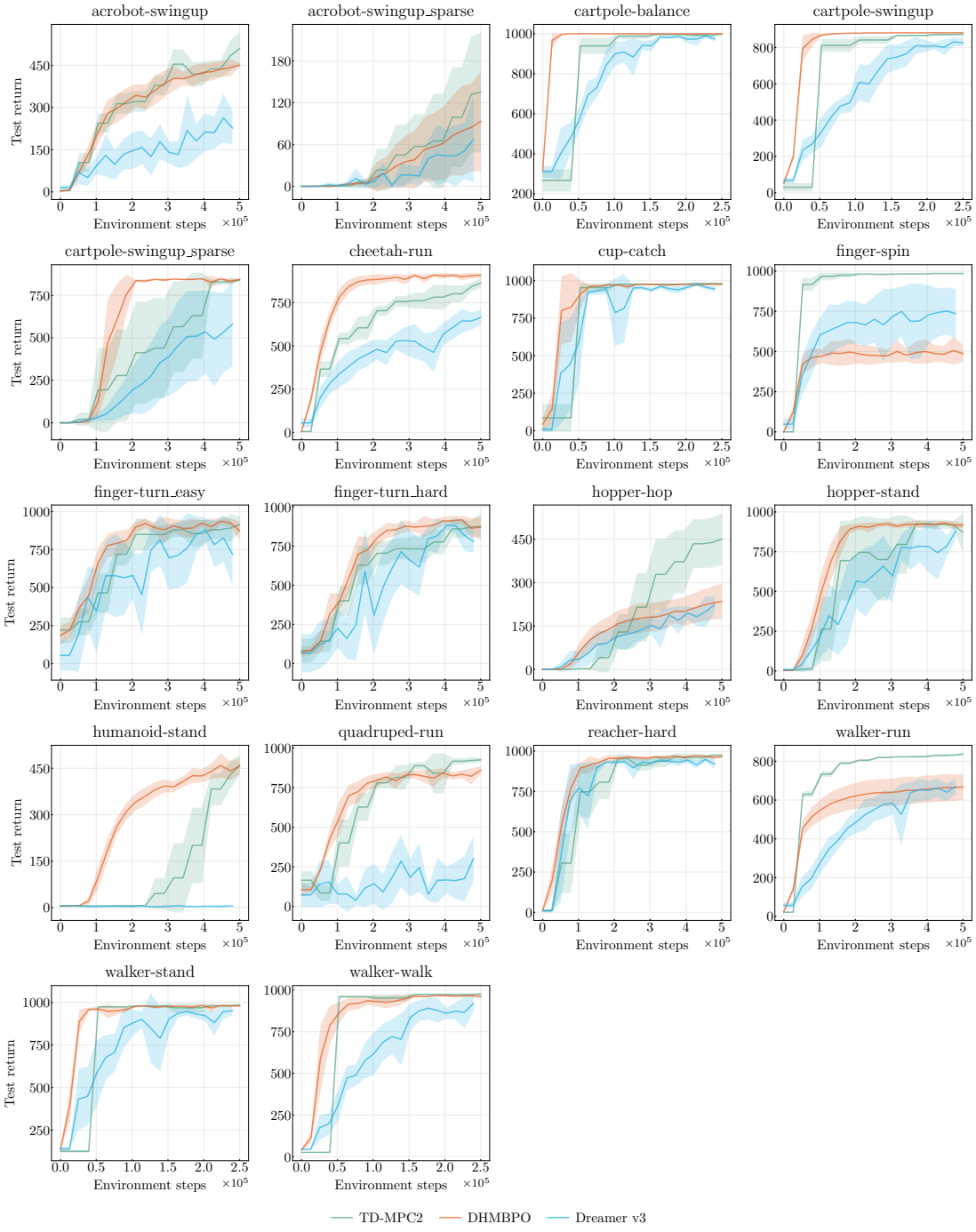

Figure 8: Comparison of sample efficiency with latent model-based methods on DMC tasks. The solid line represents the sample mean over 8 random seeds, and the shaded area indicates the 95% confidence intervals.

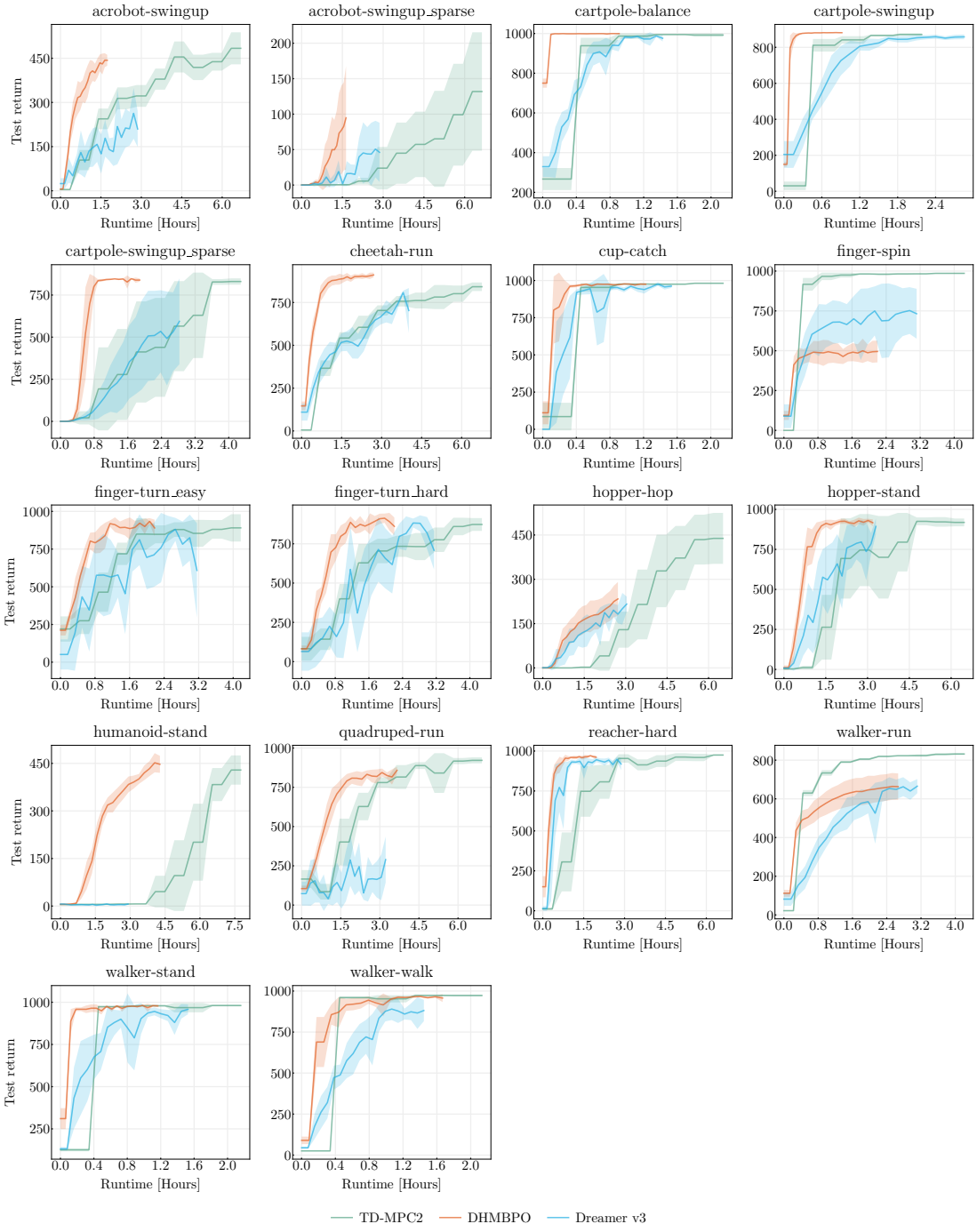

Figure 9: Runtime comparison with latent model-based methods on DMC tasks.

D Additional Experiments for Highlighting improvement over DR-based and TR-based algorithms

D.1 DHMBPO without Training Rollout but with different UTD ratios

We show the results of DHMBPO without TR but with different UTD ratios in Figure 11 for sample efficiency curves, in Figure 13 for performance profiles, in Figure 12 for runtime comparison and in Table 4 for summary

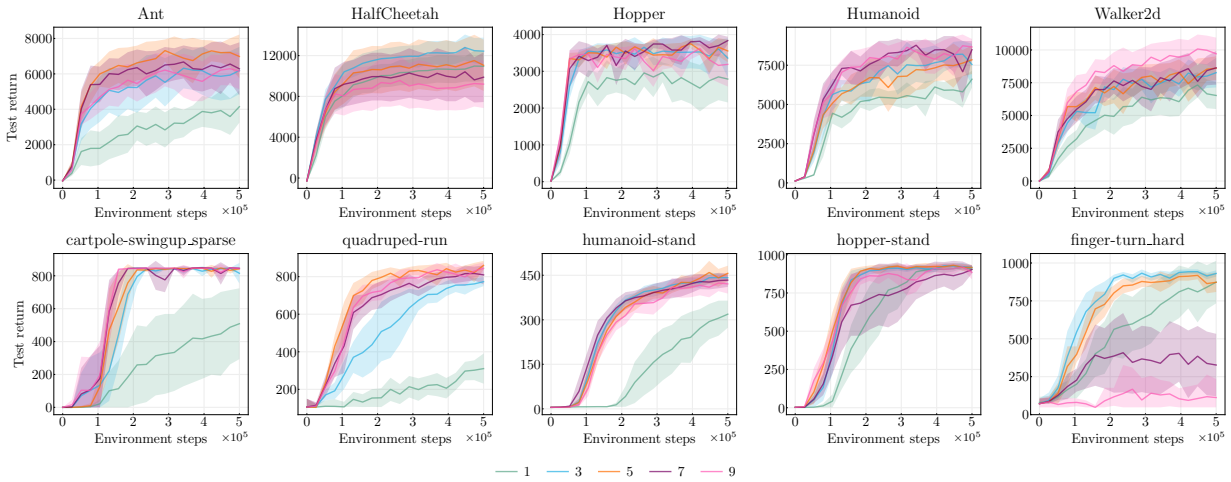

(a) Sample efficiency curves.

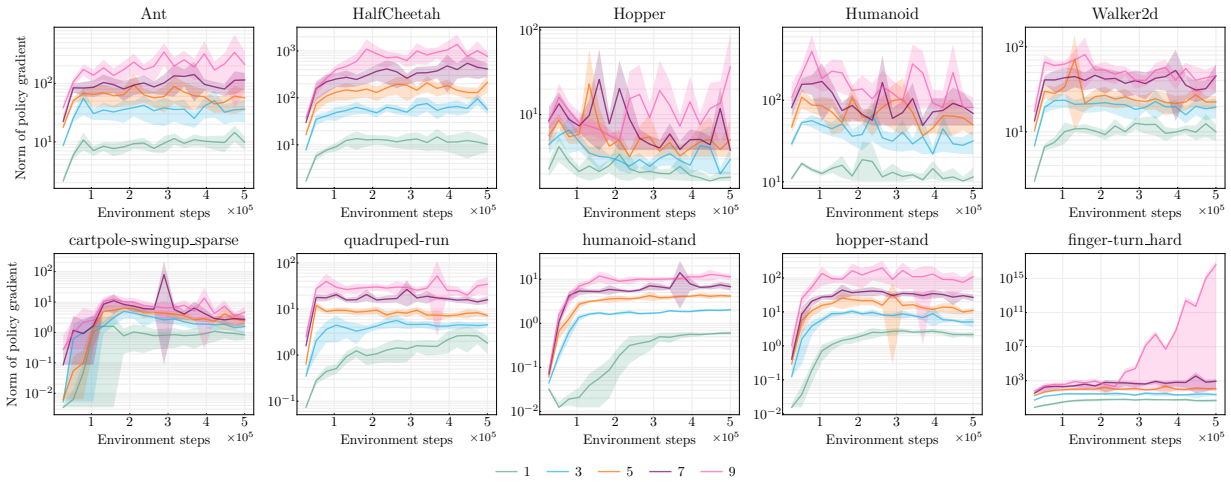

(b) Norm of policy gradient.

Figure 10: Development of test return and critic loss over environment steps.

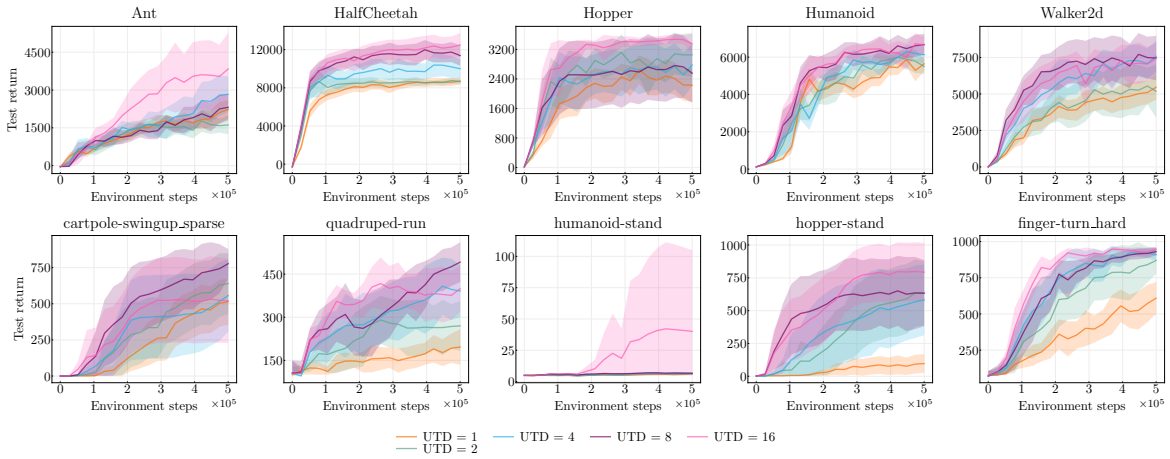

Figure 11: Sample efficiency curves of DHMBPO without TR (corresponding to MBPO) but with different UTD ratios.

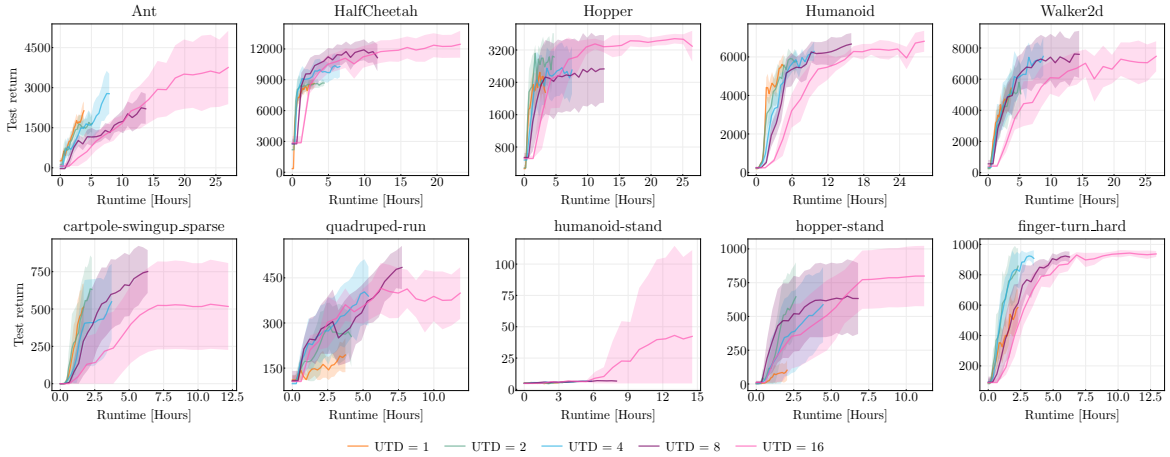

Figure 12: Runtime comparison of the DHMBPO variants without TR but with different UTD ratios.

of runtimes. We can see that the higher UTD ratio the higher performance. Conversely, DR-based algorithm, or DHMBPO without TR, needs higher UTD ratio in order to attain high sample efficiency, requiring longer runtime as shown in 12. And this results reflect that MBPO (and MACURA) were sample efficient while took so long runtime.

D.2 Trade-off in Policy Gradient Estimation

We investigate how the horizon length T of the training rollout (TR) affects the bias and variance of value gradient estimates. In principle, increasing T reduces the bias by incorporating longer reward sequences, but it can simultaneously raise the variance of the policy gradient.

Experimental Setup

For each benchmark task, we train a DHMBPO agent for 500k environment steps and then fix its policy, critic, dynamics, and reward networks, as well as the replay buffer. We draw $B = 2048$ states $\{s_b\}_{b=1}^{B}$ at random from the replay buffer. For each state s_b and each TR horizon $t \in \{1, 3, 5, 7, 9\}$, we run $R = 2048$ short-horizon rollouts under the learned model and compute the corresponding MVE-based value gradients

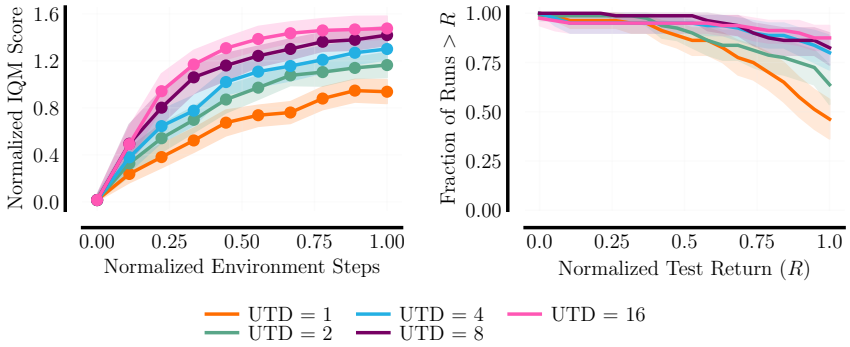

Figure 13: Performance profiles and score distributions of DHMBPO without TR (corresponding to MBPO) but with different UTD ratios. The baseline here is the variant with UTD = 1.

Table 4: Runtime until 500K environment step. Tha last row shows the ratio of mean runtime to that of the case with UTD = 1.

The UTD ratio	1	2	4	8	16
Ant	3.8	5.1	7.9	13.7	27.0
HalfCheetah	3.0	4.4	6.6	11.8	23.2
Hopper	3.3	4.7	7.5	12.6	26.5
Humanoid	4.6	6.8	9.7	15.9	28.1
Walker2d	3.6	5.2	8.7	14.5	26.7
cartpole-swingup_sparse	1.7	2.3	3.7	6.3	12.2
finger-turn_hard	2.3	2.3	3.5	6.3	12.9
hopper-stand	2.1	2.6	4.5	6.8	11.2
humanoid-stand	3.7	4.5	5.8	8.0	14.6
quadruped-run	3.8	4.2	5.4	7.7	11.9
Ratio	1.0	1.3	2.0	3.3	6.1

$\{g_{tbr}\}_{r=1}^{R}$, where g_{tbr} is a normalized vector by the dimension of policy parameter which differs across tasks. We define

$$g_{tb} := \frac{1}{R}\sum_{r=1}^{R} g_{tbr}, \quad g_t := \frac{1}{B}\sum_{b=1}^{B} g_{tb}.$$

Following the approach in our hyperparameter sensitivity analysis (Appendix C.3), we designate $t = 9 =: T$ as the ground truth horizon:

$$\bar{g} := g_T.$$

In other words, we treat the gradient computed at $t = 9$ as a baseline for evaluating shorter horizons.

To quantify bias, we measure the mean squared difference between each sample-averaged gradient g_{tb} and $\bar{g}$, averaged over all b:

$$\text{Bias}_t := \frac{1}{B}\sum_{b=1}^{B}\left\|g_{tb} - \bar{g}\right\|^2.$$

In addition, we compute the *standard error of the mean* (SEM) to capture the variability of the gradient across states in the replay buffer:

$$\text{SEM}_t := \sqrt{\frac{\sum_{b=1}^{B}\left\|g_{tb} - g_t\right\|^2}{B(B-1)}},$$

where $\|\cdot\|$ denotes the Euclidean norm over the policy parameter dimension (i.e., the gradient dimension). Intuitively, Bias_t reflects how far the sample-averaged gradient at horizon t is from the ground truth at $t = 9$, while SEM_t indicates how much variability remains across different states.

Experimental Results

Figure 14 presents results using $T = 5, 7$, and 9 as the ground-truth horizon. In all tasks except `finger-turn_hard`, we see that as t increases from 1 to 9, the bias steadily declines while the SEM grows—revealing a clear trade-off between bias and variance in the policy gradient. By contrast, in `finger-turn_hard`, the bias when T=9 did not show clear trend to decrease, suggesting the batch size of 2048 was not enough for $g_{T=9}$ to be as ground truth, and that setting $t = 5$ does not necessarily prevent gradient explosion in certain challenging domains.

Notably, all these estimates rely on a replay buffer of 2048 real-environment states, while the multiple trajectories at each state are generated by the model, although the model was trained on after 500k samples. Therefore, this method can be carried out *without* any additional real-environment interaction and used to set relatively stable length of TR horizon, as demonstrated in unclear trend of the bias in `finger-turn_hard`.

D.3 Application of DR to SAC-SVG(H) Implementation

In order to see the effect of DR on an existing implementation, we added DR procedure into the official code of SAC-SVG(H) algorithm (Amos et al., 2021), which employs the SVG method with a single GRU (Cho, 2014) as the recurrent neural network and one-step TD errors for training the critic networks. We refer to this variant as DHSAC-SVG(H) and evaluated it on five GYM tasks with varying DR lengths, repeating the execution with different 5 seeds. As shown in Fig. 15, the variants with longer DRs exhibited either poor learning performance or a drop in performance after a certain point. We investigated the training metrics and found that the critic losses started to explode as the DR length increased, as shown in Fig. 16. Here, the solid line is mean μ and shaded area shows the 95% CIs in log-scale: $\mu(1 \pm \exp(\log \text{SEM} \times 1.96))$ where $\log \text{SEM}$ is defined as $\log \text{SEM} := \sqrt{\frac{\sum_{s=1}^{S}(l_s-\mu)^2}{S(S-1)}}$ and l_s is critic loss with s-th seed.

One potential cause of these results is the deterministic nature of the model used in the SAC-SVG(H) algorithm. Predictions generated by a fixed deterministic model are likely to introduce consistent biases. In contrast, the DE model approach adopted by DHMBPO and MBPO uses multiple ensemble members, each potentially having similar biases. However, the manner in which these biases accumulate is random across ensemble members. During predictions, an ensemble member is randomly selected at each timestep, making the bias accumulation in the predicted states also random. As a result, within a single trajectory, these biases may cancel out to some extent, leading to an overall smaller average bias, albeit with larger variance.

Policy evaluation and improvement based on the higher-variance predictions of a DE model may slow down learning, but they avoid the risk of extreme predictions caused by deterministic models with large biases. On the other hand, policy evaluation and optimization using predictions with significant bias from deterministic models carry the risk of focusing on extreme values, potentially destabilizing the training process.

D.4 Comparison of Model Learning Performance

We also conducted a quantitative analysis to compare the predictive performance of models used in DHMBPO, SAC-SVG(H), and MBPO (Pineda et al., 2021), using common training and evaluation datasets.

Data Generation Procedure For each GYM task, we ran the DHMBPO algorithm for up to 500K steps. From the replay buffer, we created three input-output datasets containing data collected up to 5K, 20K, and 50K steps, respectively. Additionally, we created another dataset from all data collected between 495K and 500K steps. Each dataset was split into training (80%) and validation (20%) subsets, while the 495K–500K dataset was exclusively used for evaluation.

Evaluation Methodology For each of the three models, we trained them using the respective training datasets and measured Root Mean Squared Error (RMSE) on the training, validation, and evaluation datasets at each epoch. This procedure was repeated for three random seeds.

Results The results of the experiments are plotted separately for each dataset size, comparing training data versus validation data and training data versus evaluation data, as shown in Figs. 17– 19. Additionally, the results after 100K epochs are summarized in Table 5. The shaded areas in the plots and the ± values in the table both represent the standard error over three seeds.

D.5 Different UTD ratio

We executed DHMBPO wit the different UTD ratios, shown in Figure 20. All value for each metrics are normalized by the value for the UTD ratio = 1.

D.6 Distribution of predicted rewards and target values for critic

We applied the MBPO algorithm HalfCheetah using the MBRL-lib and created histograms of batch size rewards and critic losses calculated from the rollout buffer sampling every 10,000 interaction steps. We repeated this process up to 50,000 steps and summarized the results in Figure 21. While there are only a few outliers that can be considered as extreme values for rewards, the target values exhibit more variability, occasionally resulting in many outliers. Considering that gamma is 0.99, it can be stated that the samples at the 30,000th and 50,000th steps are extreme valued samples.

Although the causal relationship between the outliers in rewards and the anomalies in target values is not clear, it is speculated that the target values start to exhibit variability earlier than the rewards. From this observation, bounding the target critics' outputs described in Section A.5 is suggested as an effective remedy. Additionally, since the reward value can take extreme value, we use 1-st and 99-th percentiles of rewards for estimation of the lower bound and the upper bound, instead of the minimum and the maximum.

Table 5: Summary of RMSE values after 100K epochs. "Size" denotes the size of training data.

Metric	Task	Method Size	DHMBPO	MBPO	SAC-SVG(H)
Training RMSE	Ant	5000	0.29 ± 0.0	1.86 ± 0.02	1.1 ± 0.01
		20000	0.48 ± 0.0	1.21 ± 0.01	0.67 ± 0.0
		50000	0.5 ± 0.0	0.79 ± 0.02	0.59 ± 0.0
	HalfCheetah	5000	0.18 ± 0.0	1.46 ± 0.01	0.7 ± 0.01
		20000	0.35 ± 0.0	0.73 ± 0.01	0.57 ± 0.0
		50000	0.49 ± 0.0	1.58 ± 0.08	0.76 ± 0.0
	Hopper	5000	0.01 ± 0.0	0.06 ± 0.0	0.11 ± 0.0
		20000	0.02 ± 0.0	0.09 ± 0.0	0.18 ± 0.0
		50000	0.02 ± 0.0	0.04 ± 0.0	0.21 ± 0.0
	Humanoid	5000	0.44 ± 0.0	2.02 ± 0.0	2.99 ± 0.02
		20000	1.18 ± 0.0	1.99 ± 0.0	1.65 ± 0.0
		50000	1.55 ± 0.0	1.77 ± 0.01	1.69 ± 0.0
	Walker2d	5000	0.16 ± 0.0	1.74 ± 0.08	2.88 ± 0.01
		20000	0.36 ± 0.0	1.1 ± 0.01	1.48 ± 0.03
		50000	0.43 ± 0.0	0.72 ± 0.02	0.92 ± 0.0
Validation RMSE	Ant	5000	6.44 ± 0.03	4.29 ± 0.12	8.59 ± 0.07
		20000	1.51 ± 0.02	1.62 ± 0.02	3.64 ± 0.03
		50000	0.93 ± 0.01	1.07 ± 0.01	1.43 ± 0.01
	HalfCheetah	5000	3.72 ± 0.01	3.82 ± 0.03	8.78 ± 0.01
		20000	1.99 ± 0.02	1.87 ± 0.03	3.16 ± 0.05
		50000	1.61 ± 0.03	1.97 ± 0.11	3.9 ± 0.14
	Hopper	5000	0.19 ± 0.01	0.16 ± 0.01	0.25 ± 0.0
		20000	0.25 ± 0.02	0.2 ± 0.0	0.95 ± 0.03
		50000	0.13 ± 0.01	0.1 ± 0.01	1.15 ± 0.02
	Humanoid	5000	5.14 ± 0.06	5.09 ± 0.02	7.9 ± 0.1
		20000	3.25 ± 0.04	3.49 ± 0.02	9.25 ± 0.08
		50000	2.66 ± 0.01	2.52 ± 0.02	6.51 ± 0.0
	Walker2d	5000	4.08 ± 0.06	4.54 ± 0.16	6.04 ± 0.04
		20000	2.69 ± 0.02	2.79 ± 0.08	7.22 ± 0.06
		50000	1.46 ± 0.02	1.54 ± 0.03	2.49 ± 0.02
Evaluation RMSE	Ant	5000	8.61 ± 0.21	6.45 ± 0.18	10.9 ± 0.22
		20000	2.49 ± 0.06	2.05 ± 0.05	6.29 ± 0.11
		50000	1.13 ± 0.01	1.25 ± 0.01	2.61 ± 0.02
	HalfCheetah	5000	21.11 ± 0.24	274.94 ± 51.26	25.31 ± 1.15
		20000	12.76 ± 0.19	18.12 ± 1.23	16.56 ± 0.35
		50000	5.89 ± 0.06	27.91 ± 4.62	9.51 ± 0.23
	Hopper	5000	1.97 ± 0.01	20.67 ± 1.34	2.05 ± 0.03
		20000	0.99 ± 0.04	1.47 ± 0.19	1.61 ± 0.13
		50000	0.4 ± 0.0	0.62 ± 0.16	0.88 ± 0.01
	Humanoid	5000	12.91 ± 0.18	14.25 ± 0.54	17.22 ± 0.69
		20000	12.64 ± 0.21	14.63 ± 0.19	13.24 ± 0.46
		50000	11.47 ± 0.18	11.46 ± 0.17	12.86 ± 0.14
	Walker2d	5000	11.27 ± 0.28	251.58 ± 54.54	13.91 ± 0.59
		20000	11.37 ± 0.49	16.42 ± 2.58	12.38 ± 0.76
		50000	8.89 ± 0.18	22.69 ± 10.32	9.72 ± 0.3

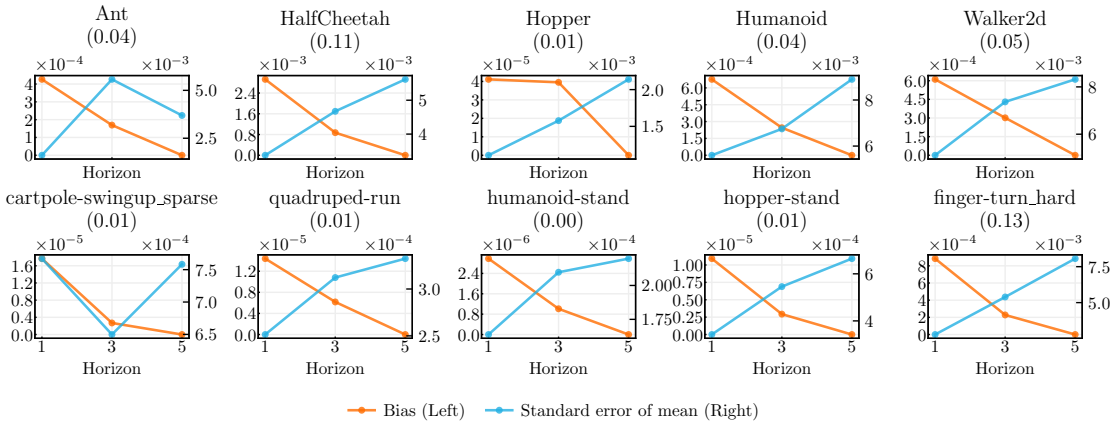

(a) T=5

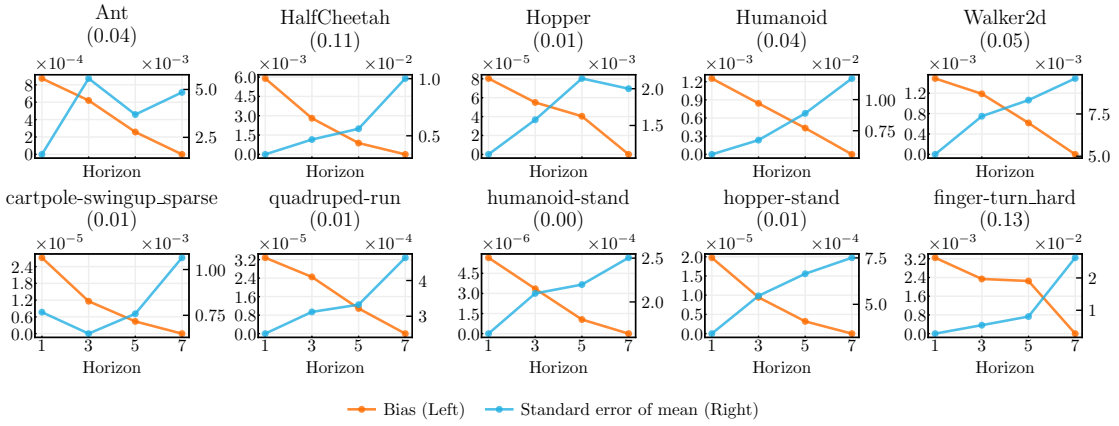

(b) T=7

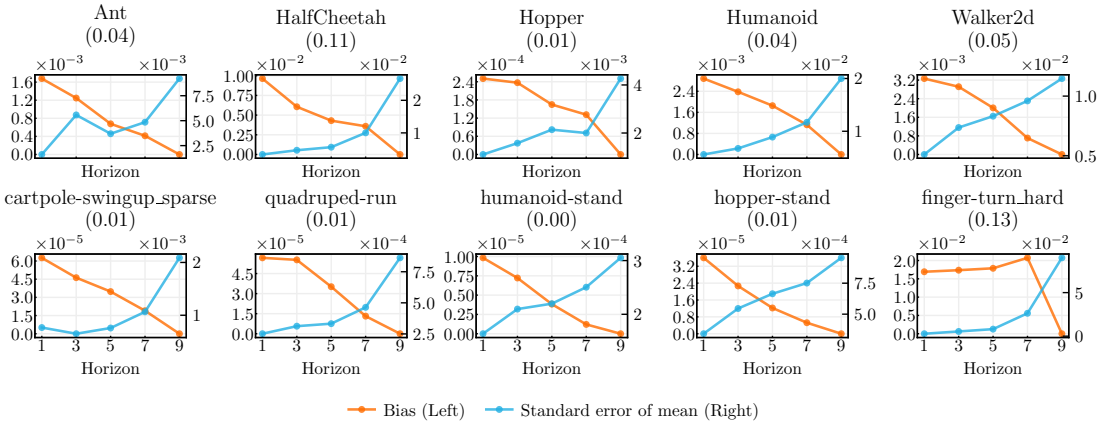

(c) T=9

Figure 14: Comparison of different ground-truth horizons. Each plot shows how the bias (left vertical axis) and SEM (right vertical axis) of the value gradient vary with the TR horizon t, using either $T = 5, 7,$ or 9 as the "ground truth" baseline ($\bar{g}$). Across all three choices of ground-truth horizon, we observe a consistent trend: the bias decreases with longer t, whereas the SEM increases.

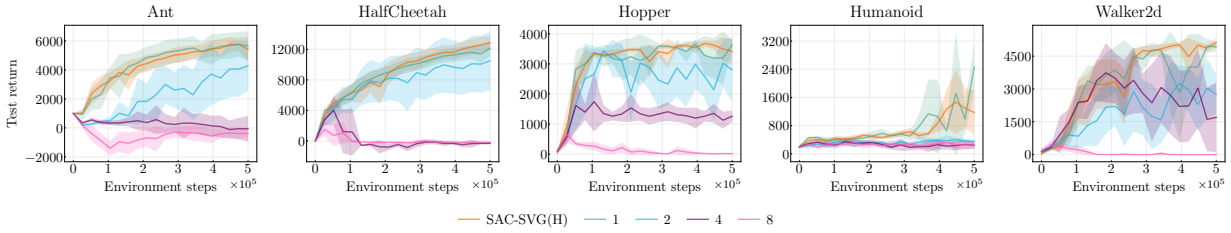

Figure 15: Sample efficiency curve of DHSAC-SVG(H).

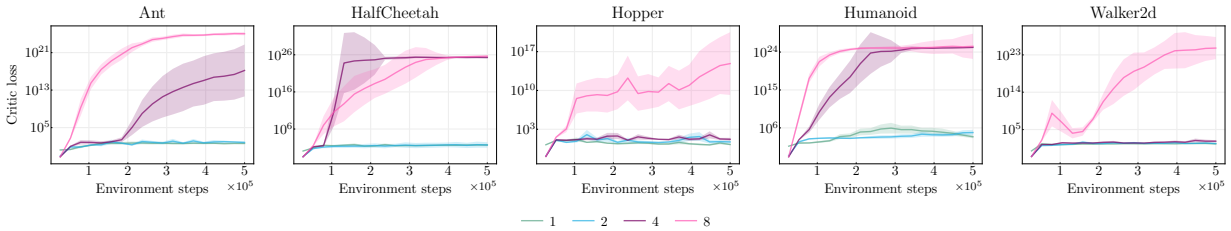

Figure 16: Development of critic loss over the number of environment steps of DHSAC-SVG(H). Solid lines is mean and shade are is for 95% CIs in log-scale. See the text in Appendix D.3 for the detail of the CIs.

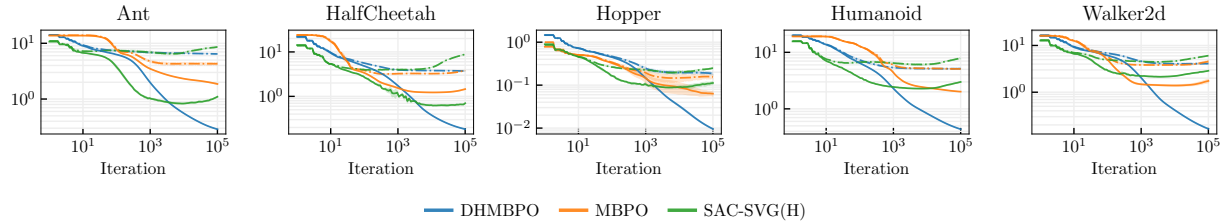

(a) Training-Validation RMSE

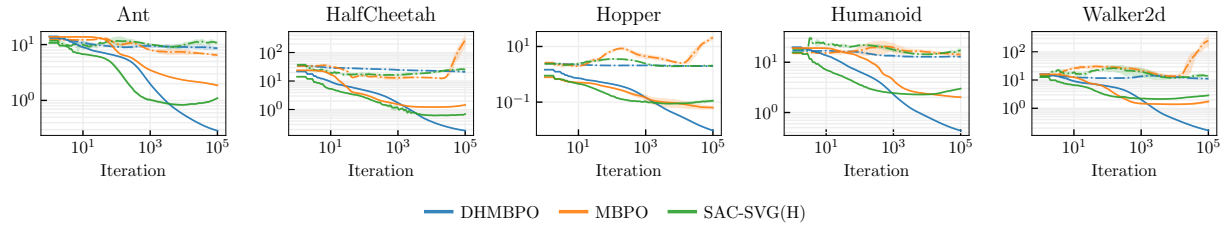

(b) Training-Evaluation

Figure 17: RMSE of model trained on 5K environment steps dataset. Solid line is for training RMSE and dashdot line is for validation RMSE or evaluation RMSE

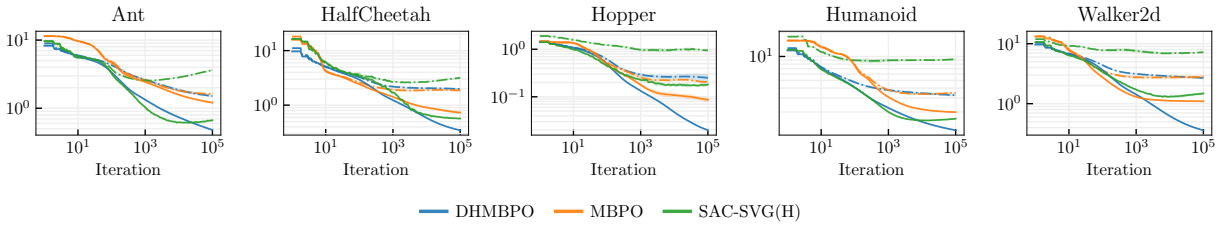

(a) Training-Validation RMSE

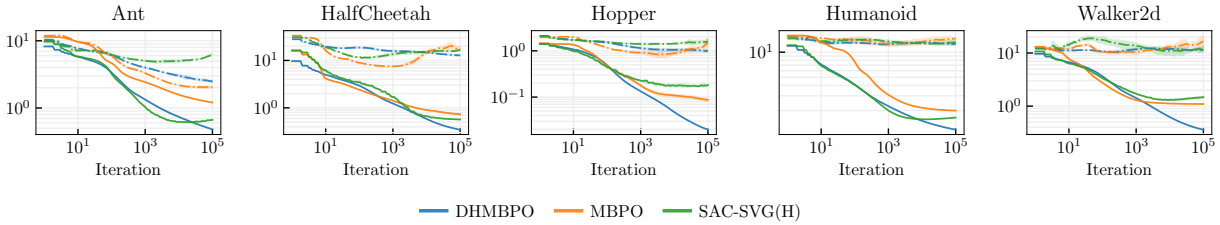

(b) Training-Evaluation

Figure 18: RMSE of model trained on 20K environment steps dataset. Solid line is for training RMSE and dashdot line is for validation RMSE or evaluation RMSE

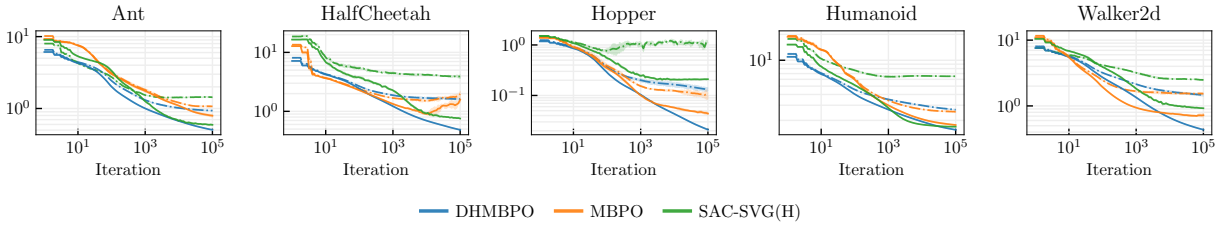

(a) Training-Validation RMSE

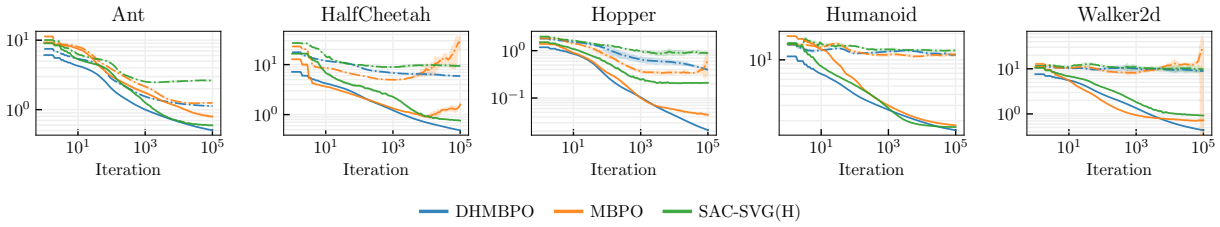

(b) Training-Evaluation

Figure 19: RMSE of model trained on 50K environment steps dataset. Solid line is for training RMSE and dashdot line is for validation RMSE or evaluation RMSE

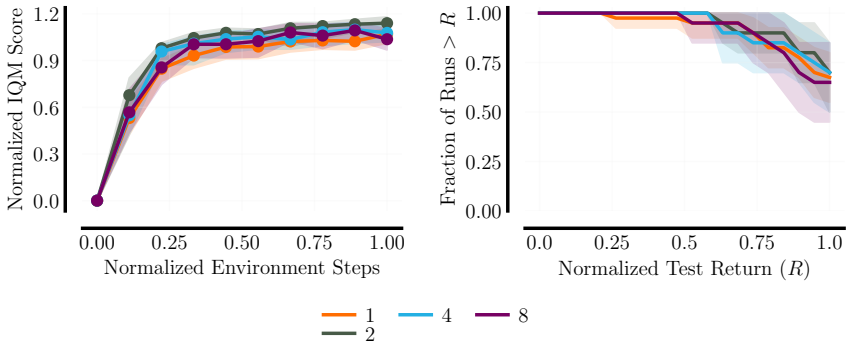

(a) Profiling plot

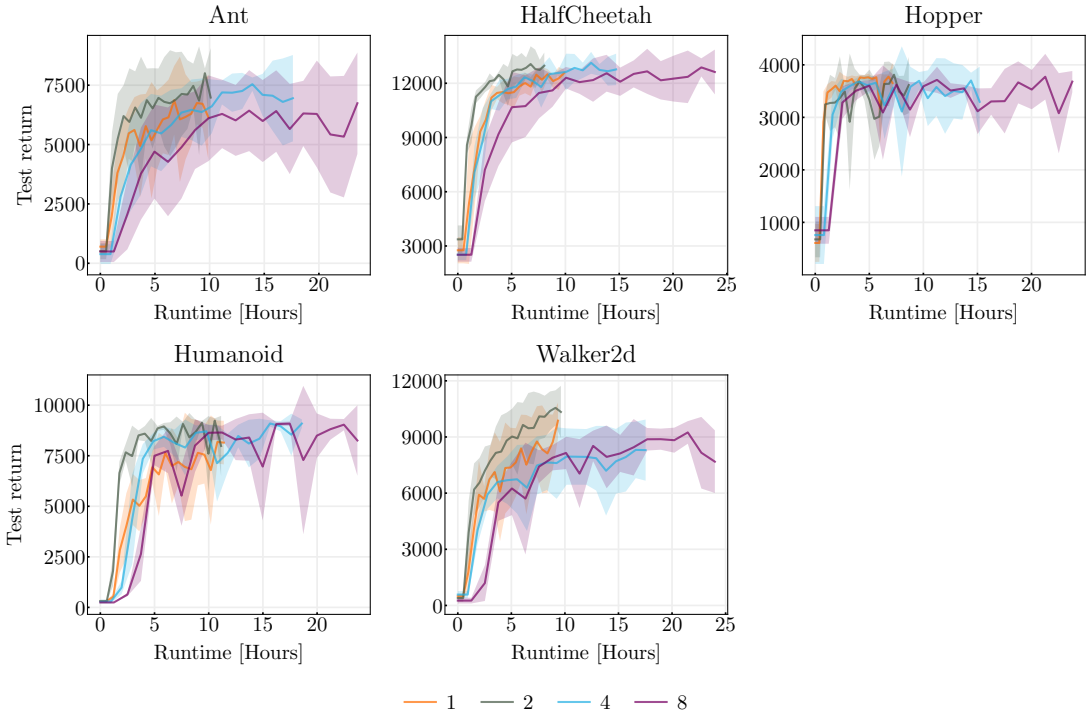

(b) Runtime

Figure 20: Results on GYM tasks of DHMBPO with different UTD ratios. Legends are for the UTD ratios

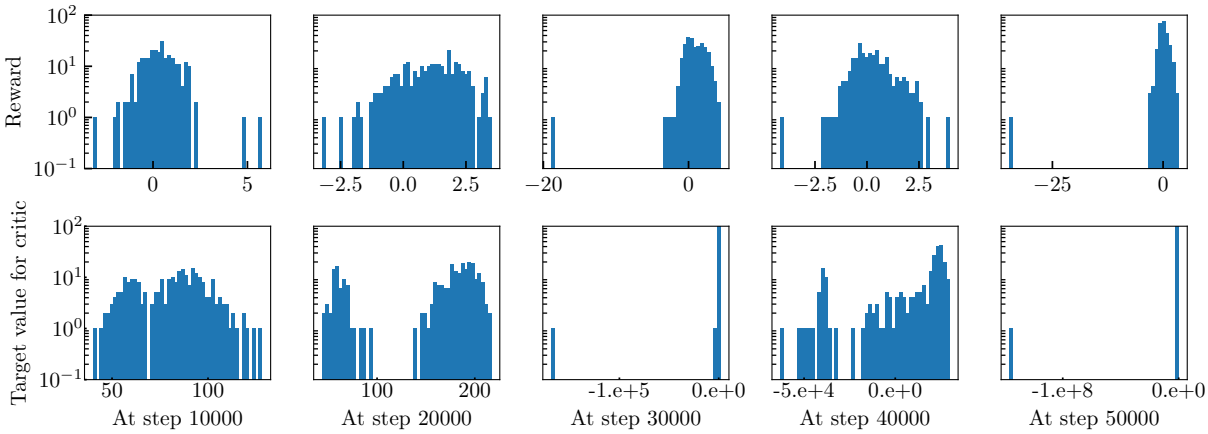

Figure 21: The transition of histograms for rewards (upper row) and target values (lower row) at every 10,000 environment steps during the execution of the MBPO algorithm on the "HalfCheetah" task. In each panel, the x-axis represents the value, and the y-axis represents the count. Noticeable outliers occur in the target values at the 30,000th and 50,000th steps.